JOURNAL OF GEOPHYSICAL RESEARCH, VOL. 114, D18112, doi:10.1029/2009JD011915, 2009

Radiative transfer in CO_2-rich paleoatmospheres

I. Halevy,[1] R. T. Pierrehumbert,[2] and D. P. Schrag[1]

Received 12 February 2009; revised 22 June 2009; accepted 29 June 2009; published 23 September 2009.

[1] Calculations of radiative transfer in CO_2-rich atmospheres are central to modeling the early climate of Earth and Mars. Line-by-line radiative transfer models are the most accurate means of carrying out such calculations and provide the basis for all other radiative transfer approaches. We examine the sensitivity of line-by-line results to three parameterizations of line and continuum absorption by CO_2, all of which yield essentially identical radiation fluxes at low CO_2 abundance. However, when applied to atmospheres containing 0.1–5 bars of CO_2, appropriate for early Earth and Mars, the outgoing longwave radiation calculated with the three parameterizations differs by as much as 40 W m^{-2}. In addition, the choice of parameters for CO_2 absorption affects the sensitivity of the calculations to infrared absorption by trace gases other than CO_2. Our findings imply that previous estimates of the amount of CO_2 required to maintain relatively warm temperatures throughout Earth's early history and during episodes in the early history of Mars are highly uncertain. Despite these uncertainties, we conclude that early Mars probably required other infrared absorbers to reach super-freezing surface temperatures, while for the early Earth, this is not necessarily the case.

Citation: Halevy, I., R. T. Pierrehumbert, and D. P. Schrag (2009), Radiative transfer in CO_2-rich paleoatmospheres, *J. Geophys. Res.*, *114*, D18112, doi:10.1029/2009JD011915.

1. Introduction

[2] The climates of Mars and Earth appear to have been relatively warm during early stages of planetary evolution. Though presently cold and arid, geomorphological, mineralogical and sedimentary evidence indicates that Mars hosted liquid surface water, at least transiently during the Noachian epoch, more than ~3.9 billion years ago (Ga) [*Baker*, 2001; *Squyres et al.*, 2004; *Poulet et al.*, 2005; *Bishop et al.*, 2008]. On Earth, the oxygen isotopic composition of zircons aged between 4.0 and 4.4 Ga suggests crystallization from magmas that incorporated rocks, which interacted with liquid surface water [*Mojzsis et al.*, 2001; *Valley et al.*, 2002; *Cavosie et al.*, 2005]. It is unclear how much liquid surface water existed in the Hadean (prior to 3.8 Ga), yet by the earliest Archean (~3.8 Ga) sediments were deposited from large bodies of water, as evidenced by metamorphosed sedimentary rocks from Isua in West Greenland [*Appel et al.*, 1998]. Reconciling this evidence with a less luminous early Sun [*Newman and Rood*, 1977; *Gough*, 1981] most likely requires that both planets had optically thicker atmospheres, which compensated for the lower solar flux and allowed the existence of relatively clement climates [*Pollack*, 1991]. A fundamental question is what atmospheres (composition and mass) could have maintained surface temperatures high enough to account for the evidence of liquid surface water early in the planetary histories of Earth and Mars. Since CO_2 is an important component of any imaginable greenhouse, resolving this question requires calculation of the radiative effect of CO_2 using radiative transfer models.

[3] In this paper we address uncertainties in radiative transfer that pervade all modeling efforts of CO_2-rich paleoatmospheres. We show that differences in the parameterization of absorption by CO_2 in line-by-line calculations, which do not adversely affect the outcome of the calculations at low CO_2 abundances, result in large differences in radiative forcing when applied to high abundances of CO_2. As few experimental data exist in the range of frequency, pressure and temperature appropriate to the earliest atmospheres of Mars and Earth, it is presently not possible to adequately parameterize absorption by CO_2 under these conditions.

1.1. Previous Work and Outstanding Questions

[4] The early climates of Earth and Mars have been extensively modeled (for a review of early work, see the study by *Pollack* [1991]). In response to improving observational, theoretical and modeling constraints, the search for a reconciliation between the geologic evidence and the existence of a weaker Sun has visited and revisited solutions involving only gaseous CO_2 and H_2O and those involving other infrared absorbers or scatterers. Because the Earth is ~1.52 times closer to the Sun than Mars, a weaker greenhouse is required to maintain super-freezing global average temperatures at any given time. *Sagan and Mullen* [1972] demonstrated that 10 ppmv of ammonia (NH_3), methane (CH_4) and hydrogen sulfide (H_2S) added to the present

[1]Department of Earth and Planetary Sciences, Harvard University, Cambridge, Massachusetts, USA.
[2]Department of Geophysical Sciences, University of Chicago, Chicago, Illinois, USA.

0148-0227/09/2009JD011915$09.00

Earth's atmosphere would have been sufficient even as far back as 4.5 Ga. However, NH_3 is highly susceptible to ultraviolet photolysis and could not have reached radiatively important concentrations in the early atmosphere, considering the likely magnitude of its natural sources [*Kuhn and Atreya*, 1979; *Kasting*, 1982]. While CH_4 and H_2S have larger natural sources, they are much less effective when added to a CO_2-H_2O atmosphere because they absorb in spectral regions where such an atmosphere is already quite opaque.

[5] These difficulties prompted solutions to the problem involving only CO_2 and H_2O vapor [*Kasting*, 1987]. A challenge to these solutions comes from upper limits on paleo-pCO_2, estimated from paleosol (fossil soil) mineral assemblages and calcified cyanobacteria [*Rye et al.*, 1995; *Hessler et al.*, 2004; *Sheldon*, 2006; *Kah and Riding*, 2007], which fall a few to several hundred times short of the pCO_2 required for habitability of the Earth throughout its history [*Kasting*, 1987]. Though there is large error associated at least with some of the paleo-pCO_2 estimates (as outlined in the study by *Sheldon* [2006]), this led to a reexamination of solutions involving other greenhouse gases, most notably methane (CH_4), as suggested by *Kasting* [1997] and *Pavlov et al.* [2000]. Following the discovery that radiative forcing by CH_4 had been overestimated because of an error, *Haqq-Misra et al.* [2008] proposed that ethane (C_2H_6), in addition to CH_4, provided the required radiative forcing. The debate is far from over; the hydrocarbon products of CH_4 photolysis under anoxic conditions scatter and absorb sunlight and have a cooling effect on the surface [*McKay et al.*, 1999; *Pavlov et al.*, 2001], the magnitude of the source of CH_4 in the deep past is uncertain [*Pavlov et al.*, 2001; *Emmanuel and Ague*, 2007] and improved calculations of the radiative effect of CO_2 have been able to meet constraints from the paleosol estimates back to ~2.7 Ga [*von Paris et al.*, 2008].

[6] The problem of maintaining liquid water at the surface of the early Earth is accentuated surrounding episodes of global, low-latitude glaciation, which occurred during the Proterozoic Eon [*Kirschvink*, 1992; *Hoffman et al.*, 1998]. During these so-called snowball events little if any liquid water was present at the planet's surface and because ice reflects much more sunlight back to space than land or ocean surfaces, high concentrations of CO_2 were required for climate recovery [*Pierrehumbert*, 2005]. Whether CO_2 was able to build up to the required concentrations over the duration of these events is uncertain [*Le Hir et al.*, 2008], reinforcing the question whether a CO_2-H_2O greenhouse is on its own capable of accounting for the evidence in Earth's geologic record.

[7] For Noachian Mars, the spatial and temporal extent of liquid surface water is unclear. Nevertheless, the predominantly Noachian distribution of dendritic valley networks, open-basin lakes and flat-floored craters with degraded rims [*Baker et al.*, 1992; *Fanale et al.*, 1992; *Craddock and Maxwell*, 1993; *Fassett and Head*, 2008a, 2008b], as well as Noachian erosion rates that are 3–6 orders of magnitude higher than Hesperian and Amazonian rates [*Golombek and Bridges*, 2000], are best explained by near-freezing surface temperatures and the action of liquid water, at least transiently. *Segura et al.* [2002, 2008] suggested that early impacts could have episodically supplied the energy required to keep the surface relatively warm, but a majority of studies explain the surface features with a more optically thick atmosphere. The greenhouse atmosphere may have been sustained by volcanic outgassing [*Phillips et al.*, 2001] or by impacts [*Zahnle*, 1993], or episodically released as internal heat triggered outflows of CO_2-saturated water [*Baker*, 2001]. Some early studies examined the effect of reduced greenhouse gases, such as NH_3, CH_4 and H_2 [*Sagan*, 1977; *Pollack*, 1979], which may have been more abundant in the early atmospheres of Mars and Earth than in their present-day counterparts. However, solutions involving these gases were hindered by the photochemical instability of NH_3, the small nonbiological source of CH_4 and the relative ease of hydrogen escape from Mars. Without infrared absorbers other than CO_2 and H_2O, the amount of CO_2 required was initially estimated to be between 5 and 10 bars [*Pollack*, 1979; *Pollack et al.*, 1987], though *Kasting* [1991] subsequently showed that no amount of CO_2 would have been enough to reach 273 K. This is because gaseous CO_2 is an efficient scatterer of solar radiation, but more importantly because CO_2 condensation decreases the atmospheric lapse rate and generates CO_2-ice clouds that scatter sunlight and cool the surface.

[8] Several ways of overcoming the problem of CO_2-ice clouds were subsequently suggested. *Forget and Pierrehumbert* [1997] proposed that the CO_2-ice clouds may have had a net warming effect because CO_2-ice clouds are much more effective scatterers of infrared radiation than water or water-ice clouds. *Kasting* [1997] suggested instead that ~1% of CH_4 in an atmosphere containing several bars of CO_2 could explain the warmer conditions, both through thermal infrared absorption and through absorption of solar radiation, which decreases the planetary albedo. Sulfur dioxide (SO_2) has been suggested in a number of studies, both as a potent greenhouse gas [*Postawko and Kuhn*, 1986; *Halevy et al.*, 2007; *Johnson et al.*, 2008] and as an absorber of ultraviolet radiation that may have prevented CO_2 condensation by heating the atmosphere [*Yung et al.*, 1997]. Here again the debate is ongoing; there is no consensus regarding the net radiative forcing by CO_2 clouds, which depends on their microphysical properties and on atmospheric dynamics [*Forget and Pierrehumbert*, 1997; *Mischna et al.*, 2000; *Colaprete et al.*, 2003], the source of CH_4 would have to be comparable to the biological source on the modern Earth, which is highly unlikely for early Mars, and SO_2 is itself susceptible to photolysis, producing reflective sulfuric acid aerosols that may counter the positive radiative forcing by SO_2.

[9] A large source of uncertainty in any modeling study of deep-time planetary climate is the surface albedo or reflectivity. Most studies, for lack of a better value, adopt the modern surface albedo, which for the Earth depends on factors such as sea level, continental configuration, ice cover on land and sea, the distribution of reflective arid regions and vegetation cover, to name a few. As these factors are increasingly difficult to constrain the farther back in time we look, the global average surface albedo during early planetary history is highly uncertain. This is even more pronounced during snowball events, when the reflectivity of ice and snow that covered Earth's surface would have been a dominant factor in the value of the

surface albedo. This value depends on many factors, such as ice thickness, cover by fresh snow, cover by dust and debris, salt and air bubble content and transient diurnal or seasonal melting, among others and varies over an enormous range between 0.5 and 0.9 [*Warren et al.*, 2002].

[10] In the case of Mars, modern bright (high albedo) regions are covered in dust containing abundant fine-grained iron oxides [*Poulet et al.*, 2007], while darker (low albedo) regions are less dusty and have surface compositions dominated by primary igneous minerals such as plagioclase and pyroxene [*Bandfield*, 2002]. In the last 20 years alone, the spatial distribution of dust cover has been observed to change, resulting in a net darkening of the surface and a simulated warming of $\sim$0.65 K globally [*Fenton et al.*, 2007]. How the dust cover changes on longer timescales is unknown. In addition, from the apparently wetter (less dusty) conditions and the likelihood of a less oxidized surface early in Mars' history [*Lammer et al.*, 2003], one might expect a lower surface albedo than the present value of 0.215, though this is little more than a guess.

[11] The outstanding questions for the early climates of Earth and Mars may be summarized as follows: (1) Can a CO_2-H_2O greenhouse account for the observations and if so, what amount of CO_2 is required? (2) In relation to the previous question, are other greenhouse gases necessary and if so, which gases are likely candidates and what amounts are required? (3) How important is the surface albedo relative to gaseous absorption? Addressing these questions requires the ability to accurately calculate radiative transfer through CO_2-rich atmospheres.

1.2. Radiative Transfer Models of Planetary Atmospheres

[12] Below we review the modeling tools used to study planetary paleoclimate and the uncertainty associated with these tools. We focus on line-by-line (LBL) calculations, which lie at the base of any other climate modeling approach, but briefly outline the uncertainty associated also with band-aggregated models (such as correlated k) and with general circulation models (GCMs). The band-aggregated models, which are more computationally efficient, use LBL results to parameterize transmission through the atmosphere and are in turn used as the radiative components in GCMs. Thus any uncertainty in the results of LBL calculations permeates into the more sophisticated climate modeling studies.

1.2.1. Absorption in Line-by-Line Calculations

[13] In LBL calculations absorption is computed on a prescribed spectral grid, at every model pressure and temperature (p and T) level and used in equations of radiative transfer to calculate upwelling and downwelling radiation fluxes. Most of the absorption arises from discrete molecular transitions or absorption lines. However, many gases, including O_2, CO_2 and H_2O vapor, exhibit far stronger and more smoothly varying absorption in some regions of the spectrum than can be accounted for by nearby absorption lines. The literature contains several explanations for this so-called continuum absorption. The explanations, which differ depending on the gas of interest and the spectral region considered, include absorption by the far wings of strong lines [*Clough et al.*, 1989; *Tipping and Ma*, 1995] and several mechanisms involving molecular collisions [*Frommhold*, 1993]. Collisions can induce absorption by momentarily allowing or creating transitions that are otherwise forbidden or nonexistent for the colliding molecules. This is achieved by altering the symmetry of the molecules, by imparting a temporary dipole on a molecule that does not normally have one, or by creating short-lived dimers with different transitions than those of the original colliding molecules [*Penner and Varanasi*, 1967]. While some continua are well understood, explanations for others, such as parts of the H_2O vapor continuum, are still the topic of debate.

[14] Practical approaches to representing continuum absorption in LBL calculations include (1) functional fits to or interpolation between experimentally determined absorption and (2) calculation of the continuum as a contribution from the very far wings of known transitions. The definition of "very far" is a matter of choice. For example, *Clough et al.* [1989] include all line absorption 25 cm^{-1} or farther from the line centers in the formulation of the continuum. To avoid double counting, this type of approach to representing the continuum is automatically related to the line cutoff distance, which is the distance from line centers out to which absorption by the lines is calculated (in the above example it is 25 cm^{-1}). Calculating the continuum as a contribution from the far wings requires adequate formulation of the absorption away from line centers, which is not easily achieved because of the difficulty in distinguishing line absorption from the continuum in experiments.

[15] Regardless of the mechanism responsible for the continuum and the way in which it is represented, the absorption coefficient, κ (in units of area per absorber amount), at a particular frequency, ν, due to a single absorbing species can be generally expressed as:

$$\kappa(\nu,p,T,x) = \sum_{|\nu-\nu_i|\le d} [\varphi(\nu,\nu_i)\cdot S_i(T)\cdot \chi(\Delta\nu_i,T)\cdot f(\Delta\nu_i,\gamma_i(p,T))] + C(\nu,p,T,x) \quad (1)$$

Such expressions are calculated for every absorber present in the model atmosphere and summed at every point on the spectral grid, at every p–T level. The sum on the right hand side is the contribution to the absorption from lines within the prescribed cutoff distance d from ν and the second term on the right hand side, $C(\nu, p, T, x)$, is the absorption that is unaccounted for by the discrete lines (continuum absorption) at ν, where x is the mole mixing ratio of the absorber. The other terms in the equation are described in the following three paragraphs.

[16] Line absorption, contrary to what its name suggests, is not monochromatic. Instead, absorption by the ith transition is strongest at the spectral location of line center, ν_i, and decays with increasing distance from that location. The decay is described in terms of a half-width, $\gamma_i(p, T)$, which is the distance from line center where the absorption is half its maximal intensity. S_i is the intensity of the transition, integrated over frequency. The values of ν_i, γ_i and S_i at reference conditions, as well as parameters required to scale them to the p and T of interest are tabulated in molecular spectroscopic databases such as HITRAN [*Rothman et al.*,

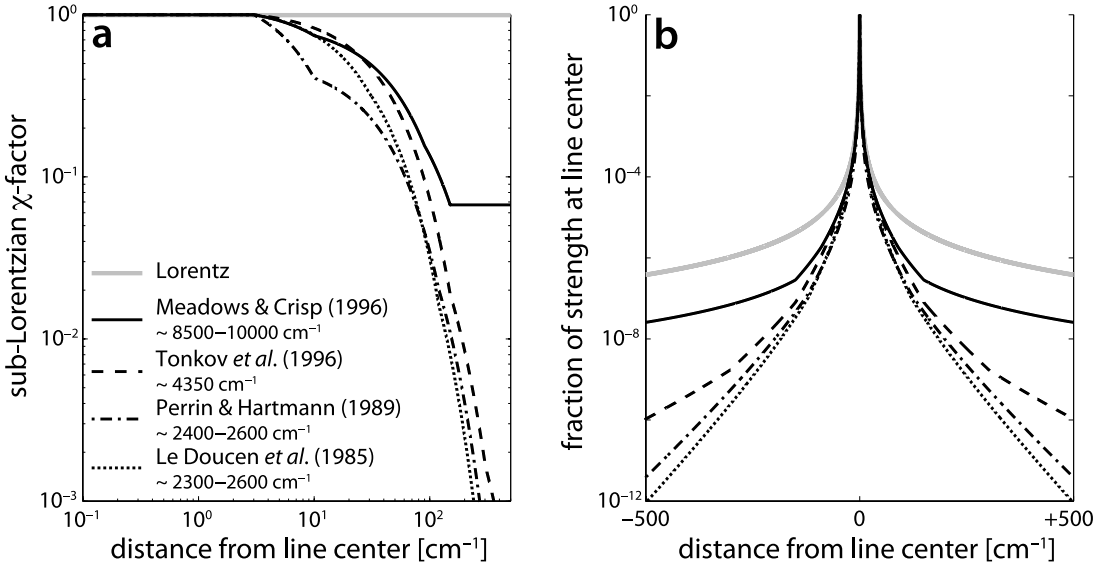

Figure 1. The effect of the χ factor on absorption by a single line. (a) Suggested χ factors for self-broadened absorption by CO_2, over the frequency regions listed in the legend [*Le Doucen et al.*, 1985; *Perrin and Hartmann*, 1989; *Meadows and Crisp*, 1996; *Tonkov et al.*, 1996]. (b) Absorption due to a single "virtual line," with a strength of unity at the line center and a half width of 0.3 cm^{-1}, multiplied by the χ factors shown in Figure 1a. The thick gray line is the unmodified Lorentz line-shape.

2005] or JPL [*Pickett et al.*, 1998]. $\Delta\nu_i$ is the difference in cm^{-1} between ν and ν_i and $\varphi(\nu, \nu_i)$ is a normalization factor, which is necessary to account for asymmetry between the absorption at frequencies higher and lower than ν_i.

[17] The nondimensional line-shape function $f(\Delta\nu_i, \gamma_i(p, T))$ describes how absorption decays with distance from the line center as a function of the half-width, γ_i. The form of f depends on the mechanism responsible for broadening the absorption line. Doppler broadening is caused by thermal motion of the molecules and is important at low pressure or very close to the line centers. A Gaussian describes this rapid decay of the absorption:

$$f_D(\nu, \nu_i) = \frac{1}{\gamma_D\sqrt{\pi}} e^{-(\Delta\nu_i/\gamma_D)^2} \tag{2}$$

where the Doppler half-width, $\gamma_D = \nu_i/c\sqrt{2k_BT/m}$, c is the velocity of light, k_B is Boltzmann's constant and m is the mass of the molecule. At higher pressure and farther away from the line center, the lines are broadened by molecular collisions and the decay in the absorption is much more gradual and can be expressed in the infrared by the Lorentz line-shape:

$$f_L(\nu, \nu_i) = \frac{\gamma_L}{\pi} \frac{1}{(\nu - \nu_i)^2 + \gamma_L{}^2} \tag{3}$$

where the Lorentz half-width, γ_L, is tabulated in spectroscopic databases, as mentioned above. The Voigt line-shape is a convolution of the Doppler and Lorentz shapes, which accurately accounts for the absorption both close to and far from the line centers. In the microwave region the Van Vleck-Weisskopf line-shape, derived assuming that the time between collisions is much longer than the duration of the collisions themselves, better accounts for the absorption [*Van Vleck and Weisskopf*, 1945]:

$$f_{VVW}(\nu, \nu_i) = \left(\frac{\nu}{\nu_i}\right)^2 (f_L(\nu, \nu_i) + f_L(\nu, -\nu_i)) \tag{4}$$

The Van Vleck-Weisskopf line-shape is equivalent to the Lorentz line-shape at higher frequencies.

[18] The requirement for the term $\chi(\Delta\nu_i, T)$ in equation (1) arises from experimental and observational evidence that absorption by CO_2 is often overestimated when calculated with a Lorentzian line-shape [*Burch et al.*, 1969; *Fukabori et al.*, 1986; *Bezard et al.*, 1990]. Multiplication of the line-shape function by this so-called χ factor results in sub-Lorentzian absorption in the far wings of the lines. For CO_2, much of the sub-Lorentzian behavior has been shown to arise from an energy redistribution process called line coupling or line mixing [*Armstrong*, 1982], though the finite duration of molecular collisions is thought to contribute as well (as opposed to the Lorentz line-shape, which is derived assuming instantaneous collisions). Recent experimental and theoretical advancements suggest that a formulation of line coupling for air-broadened CO_2 absorption [*Niro et al.*, 2004, 2005] produces sub-Lorentzian behavior that reduces and may even obviate the need for an empirical χ factor. Self-broadened absorption by CO_2 has not yet received similar treatment and still requires empirical χ factors. Several formulations of CO_2 χ factors have been suggested in the literature to account for measurements made in the spectral vicinity of different vibrational bands and at different temperatures. Some of the χ factors for self-broadened absorption by CO_2 and their effect on the line-shape are in Figure 1. A problem associated with the use of

empirical χ factors is that these have only been determined in the vicinity of some of the CO_2 bands, yet they are commonly used in radiative transfer calculations many cm^{-1} from those bands. This is undoubtedly a source of error.

[19] In contrast to CO_2, the χ factor required to account for absorption by H_2O is super-Lorentzian out to several hundred cm^{-1} from the line centers for self-broadened absorption and $\sim$100 cm^{-1} for air-broadened absorption [*Clough et al.*, 1989] and becomes sub-Lorentzian farther out. The super-Lorentzian behavior of H_2O vapor absorption has been recently modeled as due to a combination of collision-induced absorption and a line-shape component [*Clough et al.*, 2005].

[20] Though LBL calculations are regarded as the most accurate method for calculating atmospheric absorption of radiation, it is clear from the above that there are quite a few choices of parameters to be made. The values of some of these parameters, notably the χ factor, the line cutoff distance and the formulation of the continuum, if it is explicitly included, can be tuned so that the model-generated spectrum fits observational spectra. Many observations exist in the infrared under conditions relevant to current Earth, resulting in relatively good agreement between different LBL models [*Ellingson et al.*, 1991; *Tjemkes et al.*, 2003; *Kratz et al.*, 2005]. The problem is that planetary spectra of ancient Earth and Mars are obviously unavailable and experimental measurements of self-broadened continuum absorption by CO_2 between 0 and 2500 cm^{-1} and at relevant p, T and path length are rare and have not been revisited since 1971 [*Burch et al.*, 1962; *Burch and Gryvnak*, 1971; *Ho et al.*, 1971]. While theoretical formulations for the sub-Lorentzian χ factor [*Ma et al.*, 1999] and continuum absorption [*Gruszka and Borysow*, 1997] exist, there are no recent measurements to compare these formulations to. The situation in the infrared under conditions relevant to ancient Earth and Mars is somewhat analogous to the sub-millimeter spectral region under modern-day Earth conditions, where the absorption is not well constrained by observations. Indeed, *Melsheimer et al.* [2005] find in an intercomparison of several LBL models for atmospheric sounding that the choice of line-shape, continuum absorption and spectroscopic database can cause deviations of about 10% in calculation of the absorption coefficients over relatively narrow bands in the millimeter and sub-millimeter range.

[21] In summary, the results of LBL calculations for the radiative budget of early Earth and Mars are only as valid as our estimates of the unknown parameters. Here we demonstrate that three parameterizations of absorption by CO_2, two of which have proven successful in simulating an observable atmosphere (modern Earth or Venus) and all of which give comparable results for modern Earth and Mars, yield diverging results when applied to the conditions of the Archean Earth and Noachian Mars.

1.2.2. Other Infrared Absorbers

[22] Because of their low abundance, uncertainty in the formulation of absorption by trace greenhouse gases (unless it is very large) does not translate into large uncertainty in the opacity of the atmosphere and in radiative forcing. However, because an additional greenhouse gas makes a difference to the opacity of the atmosphere mostly in the regions where the atmosphere absorbs weakly (the "window regions"), the radiative effect of adding such a gas to a CO_2-rich atmosphere is influenced by uncertainties in absorption by CO_2.

[23] Interestingly, some rare isotopologues of CO_2 are analogous to trace greenhouse gases; the asymmetric isotopologues (e.g., $^{18}O^{12}C^{16}O$) have bands in the CO_2 window region (1100–1500 cm^{-1}). At high abundances of CO_2 absorption by these isotopologues can be substantial. Moreover, if the abundance of the heavy isotopes of oxygen (^{17}O, ^{18}O) were higher, absorption by the proportionally more abundant asymmetric isotopologues would be more pronounced and CO_2 would be a much better infrared absorber. In the case of Mars, the bulk isotopic composition of oxygen in the atmosphere and surface water reservoir has been affected by preferential escape of the lighter isotopes to space [*Lammer et al.*, 2008]. Water-rock interactions probably affected the oxygen isotopic composition of the surface reservoirs on both planets, though for the Earth at least, there is no agreement whether this should result in a secular change in isotopic composition or in its buffering around the present-day value [*Muehlenbachs*, 1998]. The relative abundance of hydrogen isotopes (D/H) has an analogous effect on the abundance of H_2O isotopologues and has increased with time because of preferential escape of ^1H. However, HDO has transitions where H_2O does not mostly between 2500 and 3000 cm^{-1}, a region that is unimportant for emission from early Earth and Mars, but one which may be important for a runaway greenhouse, such as that which occurred early in Venus' history [*Ingersol*, 1969; *Kasting*, 1988]. We do not know what the early values of $^{18}O/^{16}O$ and $^{17}O/^{16}O$ were, but show below that reasonable variations in these values matter little to the opacity of a CO_2-H_2O atmosphere.

[24] Whether the trace infrared absorber is another greenhouse gas or an asymmetric isotopologue of a more abundant species, it can only fill a gap in absorption inasmuch as this gap exists. This means that the sensitivity to addition of greenhouse gases other than CO_2 should differ between models with differing formulations of CO_2 line and continuum absorption.

1.2.3. Pressure Broadening Versus Scattering by N_2

[25] Because the absorption lines are broadened by collisions and because the frequency of collisions increases with pressure, at higher pressures more of the absorption by a molecular transition is shifted from the line centers to the wings. This doesn't importantly increase the transmission near the line centers where the atmosphere is highly opaque, but can significantly decrease the transmission away from line centers and result in a more strongly absorbing greenhouse. Pressure broadening by a thicker N_2 atmosphere (2–3 times present pN_2) has been recently suggested to have increased absorption by CO_2 and helped compensate for a less luminous early Sun [*Goldblatt et al.*, 2008]. A complication arises because higher pN_2 results not only in stronger positive forcing by CO_2 but also in stronger negative forcing due to Rayleigh scattering of sunlight by the N_2 itself. The magnitude of the negative shortwave forcing is linearly proportional to solar luminosity, with the implication that pressure broadening by N_2 is a more effective means of warming the Earth earlier in its history. As the added positive forcing comes from CO_2 itself, the formula-

tion of CO_2 line and continuum absorption should affect the sensitivity of the energy budget to pressure broadening.

[26] In this context, we note that trace greenhouse gases have an inherent advantage in their positive effect on the planetary radiative budget over an increase in pN_2, or for that matter, an increase in pCO_2. This is because trace absorbers have almost no impact on the planetary albedo through increased Rayleigh scattering; an atmosphere with a bar of CO_2 and 100 ppm of a trace absorber scatters shortwave radiation almost exactly like a pure 1 bar CO_2 atmosphere.

1.2.4. Uncertainty in Band-Aggregated Models and GCMs

[27] Band models are in essence variably sophisticated fits to transmission spectra generated by LBL calculations and consequently inherit the uncertainties of the latter. For computational efficiency, the spectrum is divided into bands, each of which groups together many molecular transitions. Any approach to band averaging must overcome the obstacle of accurately integrating the absorption, which is a rapidly varying function of frequency and requires many points in the integration. One way of doing this is to fit the band averaged transmission as a function of optical path, which is a smoothly varying function, instead of the absorption as a function of frequency. Examples of this approach are the Malkmus model for CO_2 and the Fels-Goody model for H_2O vapor [*Fels*, 1979]. Some of these approaches break down at high path lengths, requiring an increasing number of parameters for an adequate fit to LBL spectra. In general, the inability of empirical fits to exactly reproduce LBL-generated transmission is an additional source of inaccuracy if these methods are used.

[28] An alternative approach takes advantage of the fact the cumulative probability function of $\ln(\kappa)$ is a smooth, monotonically increasing function. An integral over the rapidly varying, frequency-dependent absorption is replaced by an integral over the cumulative probability of $\ln(\kappa)$, allowing accurate band averaging of the transmission with much fewer points in the integration than would be required if integrating over frequency. Two related methods are widely used: "exponential sums" [*Wiscombe and Evans*, 1977] and "correlated k" [*Goody et al.*, 1989]. For both methods, the distribution of the absorption coefficient is precomputed using LBL models for all the bands and at $p-T$ conditions that span the range of interest. The distributions are tabulated and then used to interpolate atmospheric absorption to the conditions of interest.

[29] Both the exponential sums and correlated k methods adequately describe the behavior of transmission over a wide range of path lengths, if p and T are close to the reference values for which the LBL absorption spectra were generated. It has been suggested that the optical thicknesses, not the absorption coefficients, are in fact the correlated property and that under certain thermodynamic conditions these methods produce large errors in the transmission [*Tvorogov et al.*, 2005]. However, in atmospheres where pressure, temperature and absorber concentrations generally decrease with altitude, a careful choice of the reference $p-T$ should keep the difference in OLR between the band models and LBL calculations to within a few percent.

[30] Finally, there is increasing use of GCMs (which employ band models as their radiative transfer components) to investigate spatial and temporal distributions of early planetary climatic parameters, which cannot be examined with the globally averaged approach of one-dimensional radiative-convective models. Although the radiative transfer components of the GCMs generally replicate LBL-generated fluxes well, the GCMs themselves differ in the way that ill understood or spatially unresolved processes are parameterized and in the magnitude (and sometimes sign) of radiative forcing supplied by various agents. An example of a spatially unresolved process that must be parameterized is small-scale convection and its effect on relative humidity and cloud radiative forcing [*Emanuel and Zivkovic-Rothman*, 1999; *Pierrehumbert et al.*, 2007]. An example of uncertain radiative forcing is that supplied by aerosols, both directly through interference with the transfer of radiation and indirectly through the effect on the distribution and physical properties of clouds [*IPCC*, 2007]. Consequently, changes in greenhouse gas concentrations and insolation, the effects of which are either damped of magnified by a complex set of feedbacks, can give rise to different net changes in radiative forcing in different GCMs.

[31] During model calibration, combinations of physical process parameterization and forcing magnitude are chosen to successfully simulate observed trends [*Kiehl*, 2007]. This ultimately leads to a relatively small range in the net radiative forcing computed by different models. For example, 20 of the GCMs used in the Intergovernmental Panel on Climate Change fourth assessment report yield a net all-sky radiative forcing between 3.39 and 4.06 W m^{-2} in response to a doubling of preindustrial CO_2 concentrations [*Forster and Taylor*, 2006]. However, this small range is due in part to a deliberate choice of parameters that are otherwise uncertain and the skill of the models outside their calibration domain is, therefore, limited. For early planetary history, when we have no clear idea of parameters such as ocean heat transport, atmospheric dust load and ice cover, among others, the results of the GCMs are highly uncertain. Furthermore, we show below that the uncertainty in gaseous absorption, which is usually considered to be low, is also very high for the conditions relevant to the early planetary history of Earth and Mars.

2. Methods

2.1. Line-by-Line Radiative Transfer Model

[32] To examine the effect of the formulation of absorption by CO_2 on the studies of early planetary climate we constructed a line-by-line radiative transfer model, described below. On a spectral grid of variable resolution in the region relevant to planetary and solar emission (0 to 60,000 cm^{-1}), we compute the absorption and scattering cross-sections of any gases present at every $p-T$ level. The cross-sections are used to calculate a composite optical depth, which is then used in equations of transfer to compute the upwelling and downwelling fluxes of diffuse and direct radiation. In order to limit our comparison to the choice of parameters for absorption by CO_2, we make the three following simplifications. First, although H_2O as well as CO_2 clouds greatly impact the surface and atmosphere energy budget, the sign and magnitude of the radiative forcing they provide depend on many factors, such as the surface albedo, the cloud top temperature, particle size, shape and density among others.

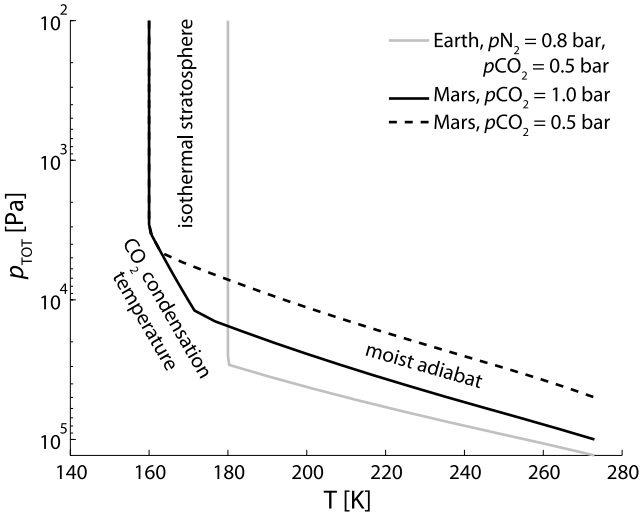

Figure 2. Sample pressure-temperature profiles for an Earth atmosphere with pN_2 of 0.8 bars and pCO_2 of 0.5 bars at the surface and for Martian atmospheres with pCO_2 of either 0.5 or 1.0 bars at the surface. An explanation of the profiles is in section 2. These profiles do not represent radiative-convective equilibrium but are instead prescribed atmospheric structures, which facilitate comparison between the opacity of the different CO_2 absorption parameterizations.

This complicated problem, which in addition requires dynamics on multiple scales, is beyond the scope of this paper and we exclude the uncertainty associated with clouds by limiting our treatment to gaseous absorption under clear-sky conditions.

[33] Second, the radiation fluxes we compute can be used to calculate atmospheric heating rates, iteratively drive the atmosphere to radiative-convective equilibrium and predict a surface temperature and an atmospheric $p-T$ structure. However, since we are interested in radiative forcing by CO_2 under comparable conditions, and since line-by-line calculations are highly time consuming, we prescribe the surface temperature and an atmospheric $p-T$ structure and compare the results of different parameterization of line and continuum CO_2 absorption for these standard conditions. For simulations of Earth's atmosphere, the temperature follows a moist adiabatic lapse rate from 273 K at the surface to an isothermal stratosphere at 180 K. This stratospheric temperature is somewhat colder than the ~220 K at the modern stratospheric temperature inversion [*Lide*, 2006], as would be expected in the absence of ultraviolet absorption by O_3. For simulations of Mars' atmosphere, we set the surface temperature to 273 K and replace the moist adiabatic temperature with the temperature of CO_2 condensation at the local pressure wherever CO_2 is saturated, following the approach of *Kasting* [1991]. The Martian stratosphere is also isothermal, with a temperature of 160 K, close to values obtained by allowing the atmosphere to reach radiative-convective equilibrium under similar conditions in previous studies [*Kasting*, 1991]. Sample $p-T$ profiles are shown in Figure 2.

[34] Third, while noting that absorption by H_2O vapor in CO_2-rich atmospheres suffers from much the same uncertainties as absorption by CO_2, we keep the formulation of absorption by H_2O constant, as described below.

2.1.1. Calculation of the Absorption

[35] The absorption cross-section (κ in $m^2\ kg^{-1}$) is calculated at every spectral grid point and $p-T$ level. Ultraviolet absorption is calculated by linear interpolation between measured absorption cross-sections from the MPI-Mainz database of molecular absorption [*Keller-Rudek and Moortgat*, 2009]. In the infrared, the absorption is calculated according to equation (1). The integrated line intensity (S_i) and self- or foreign-broadened half-width (γ_i), as appropriate, are calculated using values tabulated in the HITRAN database [*Rothman et al.*, 2005]. We use the Voigt line-shape out to 40 Doppler half-widths from line center, followed by a Van Vleck-Weisskopf line-shape farther away from the line centers and out to the chosen line cutoff distance (in cm^{-1}). We adopt a Van Vleck-Huber normalization factor [*Van Vleck and Huber*, 1977]:

$$\varphi(\nu,\nu_i) = \frac{\nu \cdot \tanh(h\nu/2k_BT)}{\nu_i \cdot \tanh(h\nu_i/2k_BT)} \tag{5}$$

where h is Planck's constant and k_B is Boltzmann's constant. We tested the sensitivity of the results to the choice of normalization factor by carrying out a few simulations with a linear normalization factor (ν/ν_i), and a quadratic normalization factor $(\nu/\nu_i)^2$, instead of the Van Vleck-Huber factor and found the effect to be negligible (see Results).

[36] The three parameter combinations for CO_2 absorption we chose to compare are listed in Table 1. These parameterizations follow approaches from the literature, two of which have been used by other workers to successfully simulate a presently observable atmosphere (Earth and Venus) and all of which yield radiation fluxes sufficiently close to those computed with the widely used radiative transfer component of the NCAR Community Climate Model, as discussed in section 2.2. The foundational support for these models is inevitably for conditions far removed from those of the early atmospheres of Earth and Mars, yet support of this kind commonly forms the justification, in the absence of better data, for the use of such models in studies of planetary paleoclimate.

[37] The first parameterization, henceforth termed "MTCKD," is fashioned after the approach of *Clough et al.* [1989, 2005], who include all absorption 25 cm^{-1} or farther from the H_2O and CO_2 line centers in the continua of these gases. This approach is employed in LBLRTM, a widely used line-by-line radiative transfer model, which successfully reproduces Earth's atmospheric spectrum and temperature structure [*Clough et al.*, 2005]. The CO_2 line-cutoff distance used in LBLRTM has not been reported in the literature and we take the value of 25 cm^{-1} directly from the code of version 11.3 of LBLRTM. The self- and foreign-broadened continua of H_2O and the foreign-broadened continuum of CO_2 were taken from version 2.0 of MT_CKD (this is the continuum available with LBLRTM and is to be distinguished from our MTCKD parameterization). The self-broadened continuum of CO_2, which is not included in MT_CKD, was taken to be 1.3 times the foreign-broadened continuum in order to account for the greater broadening efficiency of CO_2 relative to N_2, follow-

Table 1. Three Parameterizations of Line and Continuum Absorption by CO_2 Examined in This Study[a]

Parameterization				$OLR_{THIS} - OLR_{NCAR}$ (%)	
Abbreviation	Line Cutoff	CO_2 Continuum	χ Factor	1×10^3 ppmv	1×10^4 ppmv
MTCKD	25 cm^{-1}	Far wing (1)	ν-dependent	−0.14	+0.06
GBKM	500 cm^{-1}	CIA (2,3,4)	ν-dependent	+0.31	+0.68
CA	1000 cm^{-1}	None	ν-dependent	+0.35	+1.11

[a]The references in the table are the studies by (1) *Clough et al.* [2005], (2) *Gruszka and Borysow* [1997], (3) *Kasting et al.* [1984b], (4) *Moore* [1971]. For an explanation of the frequency-dependent χ factor, see the text. For all parameterizations, the line cutoff for absorption by H_2O vapor was 25 cm^{-1}, and its continuum was from *Clough et al.* [2005]. In the last 2 columns of the table is a comparison of the OLR computed by our model with the OLR computed using the radiative component of the NCAR Community Climate Model for 1,000 and 10,000 ppmv CO_2 in 1 bar of air and a constant relative humidity of 80% with altitude.

ing the approach of *Kasting et al.* [1984b]. We realize that LBLRTM and the MT_CKD formulation of the CO_2 and H_2O continua were designed to simulate present Earth's atmosphere and are here used well outside their zone of validation. However, with a self-broadened continuum formulated as described above our MTCKD parameterization produces an atmospheric opacity and an OLR essentially identical to the other two parameterizations under both foreign- and self-broadened conditions for low abundances of CO_2, as discussed in section 2.2. In addition, at high abundances of CO_2 it produces opacities intermediate between the other two parameterizations, as discussed in the Results. We therefore think that use of this parameterization to illustrate the effect of the formulation of CO_2 absorption on the outcome of early planetary paleoclimate studies is appropriate, but do not recommend its use in studies of CO_2-rich radiative transfer.

[38] The second parameterization, termed "GBKM," follows the approach of *Segura et al.* [2007], who calculate the absorption due to the lines out to distances as far as 500 cm^{-1} from line centers, modify the line-shape by the χ factor due to the study by *Meadows and Crisp* [1996] and include theoretical and experimental collision-induced CO_2 continua (CIA) from the studies of *Gruszka and Borysow* [1996, 1997, 1998] between 40 and 300 cm^{-1}, from the study of *Kasting et al.* [1984b] between 1150 and 1850 cm^{-1} (extended to the range of 1100 to 2100 cm^{-1} as in the study by *Segura et al.* [2007]; D. Crisp, personal communication, 2008) and from the study of *Moore* [1971] between 4000 and 4600 cm^{-1}. The third parameterization, termed "complete absorption" and abbreviated "CA," is modeled after the approach of *Meadows and Crisp* [1996], who do not include an explicit CO_2 continuum. They account for the background absorption by calculating line absorption, modified by a χ factor appropriate for the spectral region considered, out as far as 1000 cm^{-1} from the line centers. This approach successfully simulated the observed spectrum of Venus between 1 and 1.3 μm.

[39] As mentioned above, different χ factors have been found necessary to account for observations made at different frequency regions. Therefore, for all three parameter combinations we adopt a "frequency-dependent" χ factor, which is just an extrapolation from the spectrally closest available empirical formulation of the χ factor to the frequency of interest. We take this approach for lack of more complete data, noting that extrapolation of empirical χ factors far away from the band for which they were formulated undoubtedly introduces errors. The χ factor we used for self-broadened absorption by CO_2 is from the study of *Le Doucen et al.* [1985] at frequencies lower than 2300, followed by the χ factor from the study of *Perrin and Hartmann* [1989] at frequencies between 2300 and 3000 cm^{-1}, from the study of *Tonkov et al.* [1996] between 3000 and 6000 cm^{-1} and from the study of *Meadows and Crisp* [1996] at frequencies higher than 6000 cm^{-1}. The χ factor for foreign-broadened absorption by CO_2 is equivalent to the line-coupling approach by *Niro et al.* [2005] up to a frequency of 2000 cm^{-1} and from the study of *Perrin and Hartmann* [1989] for higher frequencies. Our parameterizations thus differ somewhat from the approaches after which they are fashioned, which usually adopt one formulation of the χ factor. It is noteworthy, however, that at the emitting temperatures of both early Earth and Mars, the choice of χ factor (or almost any other parameter for that matter) at frequencies greater than 2500 cm^{-1} matters little to the opacity of the atmosphere to outgoing longwave radiation.

[40] To allow comparison of the chosen parameterizations for absorption by CO_2, and despite uncertainty in absorption by H_2O vapor in CO_2-rich atmospheres [*Kasting et al.*, 1984a], we kept the parameterization of absorption by H_2O vapor fixed in all three cases. The line cutoff for H_2O was 25 cm^{-1} and its continuum from the study of *Clough et al.* [2005].

2.1.2. Equations of Transfer

[41] In combination with the absorption cross-section, κ, a scattering cross-section, σ (in m^2 kg^{-1}), is calculated for each of the gases in the atmosphere according to Rayleigh theory and used to calculate the combined optical depth (τ) due to both molecular absorption and scattering.

$$\frac{d\tau}{dp} = -\frac{1}{g}\sum_i q_i \cdot (\kappa_i + \sigma_i) \tag{6}$$

g is the gravity of the planet, q_i is the mass mixing ratio of the absorber/scatterer and the sum is over the gases present in the model atmosphere. The optical depth, which increases from a value of zero at the surface to τ_∞ at the top of the atmosphere, is used to solve the two-stream equations for diffuse radiative transfer at every frequency on the prescribed spectral grid.

$$\frac{dI_+}{d\tau} = \beta_2 I_- - \beta_1 I_+ + \beta_B \pi B(T(\tau)) + \beta_+ L_\odot e^{-\frac{\tau_\infty - \tau}{\cos\zeta}} \tag{7}$$

$$\frac{dI_-}{d\tau} = \beta_1 I_- - \beta_2 I_+ - \beta_B \pi B(T(\tau)) - \beta_- L_\odot e^{-\frac{\tau_\infty - \tau}{\cos\zeta}} \tag{8}$$

I_+ and I_- are the upwelling and downwelling fluxes of diffuse radiation, respectively. B is Planck's function, $L_\odot$ is the incoming solar radiation and ζ is the zenith angle. The β_js are rate coefficients describing the attenuation of radiation due to scattering and absorption.

$$\beta_1 = \beta \cdot (1 - \hat{g}\omega_0) + \beta' \cdot (1 - \omega_0) \quad (9)$$

$$\beta_2 = \beta \cdot (1 - \hat{g}\omega_0) - \beta' \cdot (1 - \omega_0) \quad (10)$$

$$\beta_B = 2\beta' \cdot (1 - \omega_0) \quad (11)$$

$$\beta_+ = \omega_0/2 - \beta\omega_0\hat{g}\cos\zeta \quad (12)$$

$$\beta_- = \omega_0/2 + \beta\omega_0\hat{g}\cos\zeta \quad (13)$$

ω_0 is the single scattering albedo and $\hat{g}$ characterizes the asymmetry of the scattering. In this study, scattering by the gases of interest is symmetric and $\hat{g}$ is equal to zero, but this formulation allows use of the model to compute the radiative effect of asymmetric scatterers, such as clouds or aerosols. The value of β and β' depends on the angular distribution of radiation. A hemispherically isotropic approximation (β = 0.75, β' = 1) was used for radiation in the thermal infrared and an Eddington approximation ($\beta = \beta' = 1$) for shorter wavelengths.

[42] The boundary conditions are

$$I_-(\tau = \tau_\infty) = 0 \quad (14)$$

$$I_+(\tau = 0) = A_s \cdot \left(I_-(\tau = 0) + L_\odot e^{-\frac{\tau_\infty}{\cos\zeta}}\right) + \pi B(T_s) \quad (15)$$

where A_s is the surface albedo at ν and T_s is the surface temperature. Most of the calculations were limited to the thermal infrared and microwave (0–2500 cm^{-1}), where A_s was taken to be zero. As mentioned above, we do not know the value of the visible to near-infrared A_s of early Earth or Mars. However, in calculations demonstrating the importance of A_s to the results we adopted a spectrally invariant value of 0.215 for Mars and values between 0.6 and 0.8 for a globally glaciated Earth. The boundary conditions above specify that there is no diffuse downwelling flux at the top of the atmosphere (equation (14)), and that the diffuse upwelling flux at the surface consists of the reflected diffuse downwelling flux, the reflected solar flux and blackbody radiation at T_s (equation (15)).

[43] We obtain global average upwelling and downwelling radiation fluxes by solving equations (7) and (8) at values of the zenith angle (ζ) between 0 and 90 degrees, in increments of 5 degrees and integrating the results.

2.2. Model Validation

[44] We carried out simulations with a spectral resolution between 0.01 and 1 cm^{-1} and found that up to and including a resolution of 1 cm^{-1} in the thermal infrared and microwave (0–2500 cm^{-1}) the OLR was within ±0.6% of the value calculated with a resolution of 0.01 cm^{-1}. For all of the simulations described below we used a spectral resolution of 0.5 cm^{-1}, for which the error relative to the high-resolution simulation was less than 0.2%.

[45] The longwave performance of our model relative to the radiative component of the NCAR Community Climate Model is shown in Table 1. The OLR computed by our model under all three parameterizations comes within ±1.11% of the OLR computed by the NCAR model up to CO_2 concentrations as high as 10,000 ppmv. This is slightly higher than the 1% range in OLR found in an intercomparison of LBL models [*Ellingson et al.*, 1991], but not unexpected because the CO_2 concentrations in the validation runs are more than two orders of magnitude higher than in the intercomparison mentioned. In addition to the simulations presented in Table 1, we simulated a dry mock-Martian atmosphere with $p$$CO_2$ of 6.5 millibar at the surface. The objective of these simulations was to compare the performance of the three parameterizations under conditions of self-broadened CO_2 absorption, with no H_2O vapor that can decrease the differences in opacity between the parameterizations. For the mock-Martian simulations we prescribed an identical atmospheric p–T structure for all three parameterizations, with a surface temperature of 240 K and tropospheric temperature decreasing adiabatically down to an isothermal stratosphere at 140 K. The difference in the computed OLR between the parameterizations is ~0.1%. From the comparison with the NCAR Community Climate Model and the intercomparison between the parameterizations under pure CO_2, mock-Martian conditions, we conclude that all three parameterizations successfully simulate radiative transfer through atmospheres with low CO_2 abundances. We show below that when applied to the conditions relevant to early Earth and Mars the results diverge.

3. Results

3.1. Pure CO_2 and CO_2 + N_2 Simulations

[46] For the parameterizations listed in Table 1, we simulated: (1) a dry Earth atmosphere with $p$$N_2$ of 0.8 bars, and $p$$CO_2$ of 0.1, 0.2, 0.3, 0.5 and 0.8 bars at the surface, (2) a dry Martian atmosphere with $p$$CO_2$ of 0.5, 1, 2, 3 and 5 bars at the surface. In all cases, the atmosphere consisted of 40 logarithmically spaced p levels and the T profile was as described in section 2. Since the formulation of scattering is similar in all three parameterizations, the shortwave parts of the simulations did not give rise to differences in radiative forcing. This was not the case in the mid and far infrared, however, as summarized in Figures 3a–3c. The GBKM parameterization consistently yielded the lowest OLR, followed by the MTCKD parameterization and finally the CA parameterization. Figure 3c shows that the difference in OLR between the least opaque and most opaque parameterizations ($OLR_{CA} - OLR_{GBKM}$) increases with increasing $p$$CO_2$ over the range relevant to early Earth and Mars.

[47] The effect of the different formulation of absorption in the CO_2 window regions is demonstrated in Figures 4a–4c, where the absorption coefficient (κ), the radiating temperature (T_{rad}) and the cumulative OLR are shown as a function of frequency for a dry Martian case with $p$$CO_2$ of 1 bar at the surface. As shown in panel a, the three parameterizations yield nearly identical κ near the CO_2 tran-

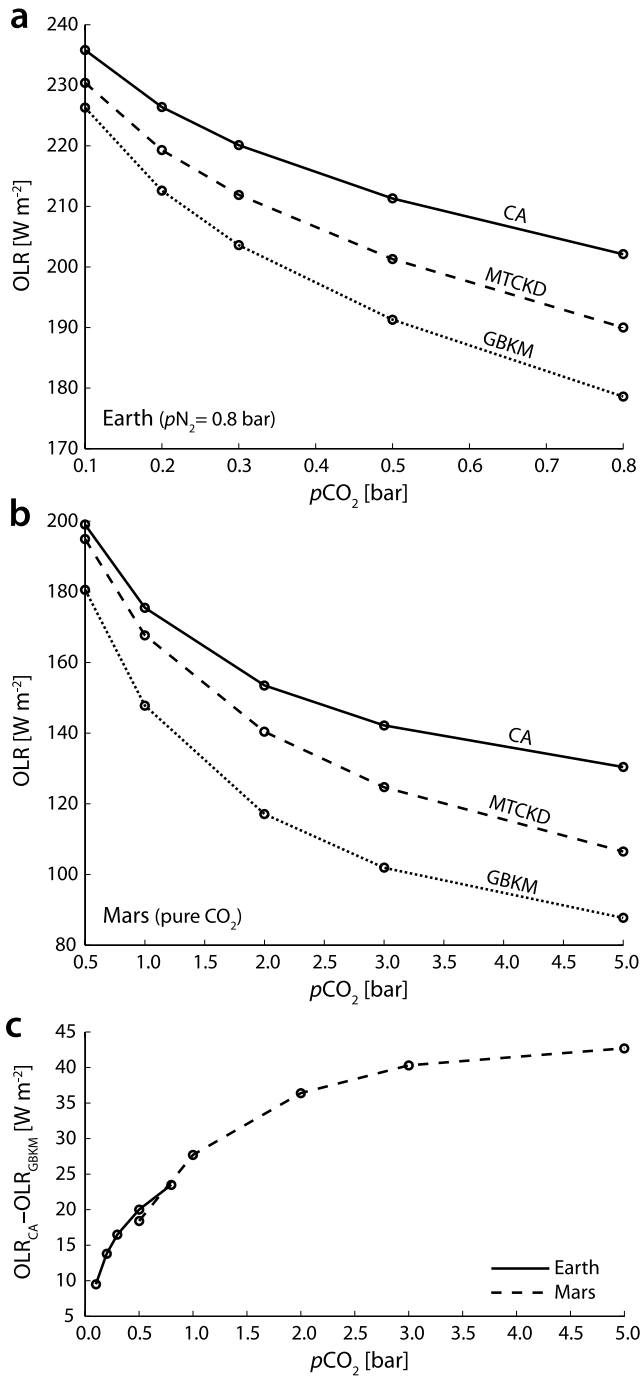

Figure 3. Outgoing longwave radiation (OLR) as a function of the surface partial pressure of CO_2 (pCO_2) for the three parameterizations. (a and b) Simulations of Earth and Mars, respectively. The details of the simulations are in section 3. Since the atmosphere was not driven to radiative-convective equilibrium, the OLR does not realistically represent emission from planets' surfaces but is intended to provide a comparison between the parameterizations. (c) Difference in OLR between the CA and GBKM parameterizations growing as pCO_2 is increased.

sitions. Below 500 cm^{-1} and between 1200 and 1800 cm^{-1}, however, differences in the formulation of the absorption lead to coefficients that differ by as much as about five orders of magnitude (with an exception in the region around 1300 cm^{-1}, where all three parameterizations are identically opaque because of bands of the asymmetric isotopologues of CO_2). Panels d–f are the same as panels a–c but with a constant relative humidity of 80%. Note that the combined absorption coefficient of CO_2 and H_2O vapor is in units of m^2 per kilogram of a gas mixture with the relative concentrations of CO_2 and H_2O at the 100 millibar level. Absorption by water vapor decreases the differences in κ calculated under the three parameter combinations below 500 cm^{-1} and above 1500 cm^{-1}. In the dry and moist case, the differences in κ between the parameterizations lead to different rates of OLR accumulation with integration over frequency, as shown in panels c and f and discussed later.

[48] To examine the balance between the opposite effects of pressure broadening and Rayleigh scattering by N_2, we simulated a dry Earth atmosphere containing 1.5 and 2.0 bars of N_2 instead of the nominal 0.8 bars. We included the far infrared and microwave collision-induced absorption due to N_2–N_2 pairs [*Boissoles et al.*, 1994, 2003], because this is a pN_2-dependent component of the absorption that may be important in the absence of H_2O vapor. The results are shown in Table 2. Increasing pN_2 to 1.5 bars causes a net decrease in radiative forcing for the CA parameterization (−1.6 W m^{-2}) and only a modest increase in radiative forcing for the MTCKD and GBKM parameterizations (2.6 and 1.7 W m^{-2}, respectively) if solar luminosity is 75% its present value, as in the early Archean [*Gough*, 1981]. Because of the dependence of the negative forcing due to Rayleigh scattering on the solar flux, the net forcing for the MTCKD and GBKM parameterizations changes sign if solar luminosity is equal to or greater than about 101% and 92% of its present value, respectively (which would occur around 0.07 Gyr from today and 1.02 Ga, respectively). Increasing pN_2 to 2.0 bars, again causes a net decrease in radiative forcing for the CA parameterization (−3.2 W m^{-2}) and an increase in radiative forcing for the MTCKD and GBKM parameterizations (3.5 and 1.8 W m^{-2}, respectively) for 75% present solar luminosity. For this value of pN_2 the net forcing changes sign at or above about 97% and 86% present solar luminosity, respectively (which would occur around 0.34 and 1.88 Ga, respectively). The maximal effect of leaving out the collision-induced absorption due to N_2–N_2 pairs is only a 0.5 W m^{-2} reduction in net radiative forcing (for the CA parameterization at pN_2 of 2.0 bars). In an atmosphere containing H_2O vapor the N_2–N_2 continuum would matter even less.

3.2. Normalization Factor and the χ Factor

[49] As mentioned in section 2, to account for the apparent frequency dependence of the χ factor we followed recommendations from different studies in different frequency regions. To adopt a single χ factor over the entire spectrum despite the existence of better suited values for specific frequency regions would be introducing unnecessary error. However, to demonstrate the importance of the choice of χ factor we carried out simulations with the most strongly and most weakly sub-Lorentzian formulations. For self-broadened absorption by CO_2 these are the χ factors due to the studies by *Perrin and Hartmann* [1989] and *Tonkov et al.* [1996], respectively (Figure 1). The simulations were for a dry Martian atmosphere with pCO_2 of 1 bar

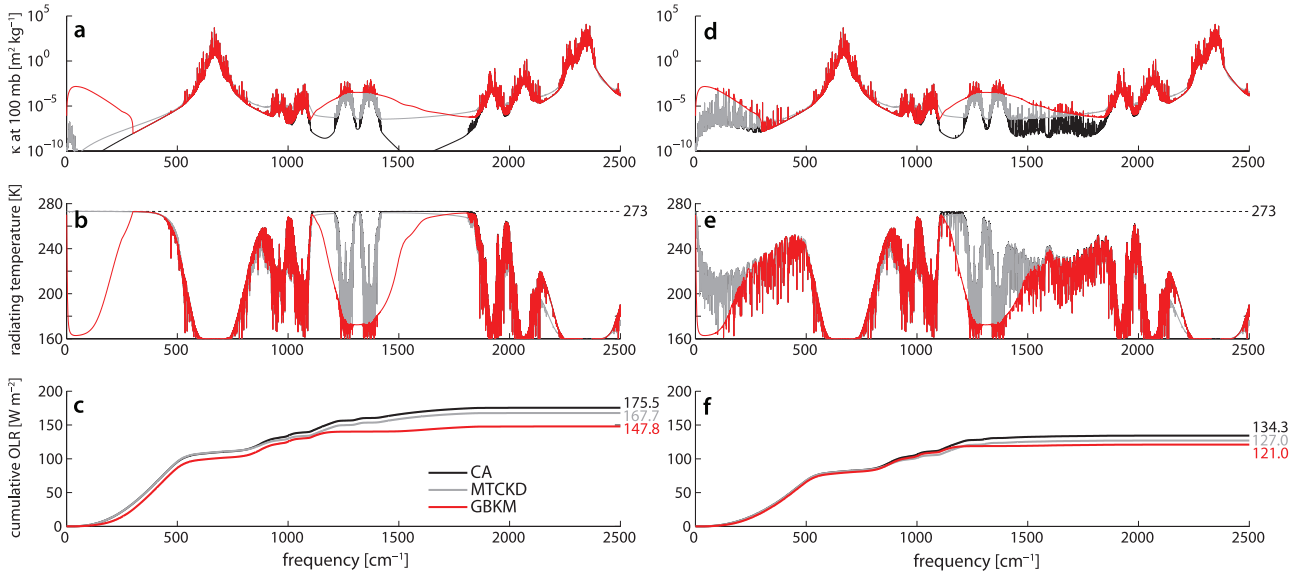

Figure 4. The effect of different CO_2 line and continuum parameterization on atmospheric opacity in LBL calculations. The three graphs on the left are for Martian gravity and a pure CO_2 atmosphere with a surface pressure of 1 bar, while in the three graphs on the right H_2O vapor was added, at an altitude-constant relative humidity of 80%. (a and d) Absorption coefficient (κ in m^2/kg of the gas mixture) at 100 mb, including contributions from the lines and the continuum. (b and e) Radiating temperature as a function of frequency. This is a measure of the opacity of the atmosphere, with more opaque regions emitting at a temperature closer to the stratospheric temperature (160 K) and more transparent regions emitting closer to the surface temperature (273 K), which is marked with a dotted line. The parameterization used strongly affects the opacity of the atmosphere in the frequency regions below 500 cm^{-1} and between 1200 and 1800 cm^{-1}. (c and f) Cumulative OLR as a function of frequency. The numbers to the right of Figures 4c and 4f are the total values of OLR (W m^{-2}), over the frequency interval 0–2500 cm^{-1}, for the three parameterizations. In the pure CO_2 case (Figures 4a, 4b, and 4c), the main difference between the parameterizations is the rate of OLR increase below 500 cm^{-1} and between 1200 and 1500 cm^{-1}; the GBKM parameterization is substantially more opaque in these regions and OLR increases less than for the other two parameterizations. In the cases with a relative humidity of 80% (Figures 4d, 4e, and 4f), water vapor increases the opacity of the region below 500 cm^{-1} and the OLR of the three parameterizations significantly diverges only beyond 1200 cm^{-1}.

at the surface and the results are as follows. For the CA parameterization, the OLR is 177.7 and 168.5 W m^{-2} with the χ factors due to the studies by *Perrin and Hartmann* [1989] and *Tonkov et al.* [1996], respectively, compared with 175.5 W m^{-2} computed with the nominal frequency-dependent χ factor. The corresponding values for the GBKM parameterization are 150.1 and 141.0 W m^{-2} (compared with 147.8 W m^{-2}) and for the MTCKD parameterization they are 167.7 and 167.6 W m^{-2} (compared with 167.7 W m^{-2}). Thus, the strongly sub-Lorentzian χ factor resulted in an OLR about 9 W m^{-2} higher than the weakly sub-Lorentzian χ factor for the CA and GBKM parameterizations, while the MTCKD parameterization was insensitive to the change (a difference of less than 0.1 W m^{-2}). We elaborate on this in the Discussion.

[50] Additionally, we carried out simulations with linear and quadratic normalization factors instead of the Van Vleck-Huber normalization factor, as mentioned in section 2. The simulations were again for a dry Martian atmosphere with pCO_2 of 1 bar at the surface. The linear and quadratic normalization factors yielded maximal differences in OLR of less than 0.21 and 0.19 W m^{-2}, respectively (out of about 175 W m^{-2}). These differences

Table 2. Differences in Top-of-Atmosphere Longwave and Shortwave Radiative Forcing (W m^{-2}) Between Earth Atmospheres With pN_2 of 1.5 and 2.0 Bars and pCO_2 of 0.5 Bars, Relative to the Standard Case (pN_2 = 0.8 Bar, pCO_2 = 0.5 Bars)[a]

	pN_2 = 1.5 bars				pN_2 = 2.0 bars			
Parameterization	Δ_{LW}	Δ_{SW}	Δ_{net}	t (Ga)	Δ_{LW}	Δ_{SW}	Δ_{net}	t (Ga)
MTCKD	+10.2	−7.6	+2.6	−0.07	+15.4	−11.9	+3.5	0.34
GBKM	+9.3	−7.6	+1.7	1.02	+13.7	−11.9	+1.8	1.88
CA	+6.0	−7.6	−1.6	N/A	+8.7	−11.9	−3.2	N/A

[a]The difference in shortwave forcing was calculated assuming solar luminosity 75% its present value (~3.8 Ga). The rightmost column for each case of pN_2 shows the time (Ga) from which the increase in scattering due to the higher pN_2 is equal to or greater than the additional longwave forcing from pressure broadening of CO_2 line absorption (i.e., the time from which the higher pN_2 cools the surface instead of warming it).

are smaller than the error resulting from the spectral spacing used in the integration over frequency.

3.3. Other Infrared Absorbers

[51] We included 1, 10, 100 and 1000 ppmv of CH_4, N_2O, NH_3, SO_2 and H_2S in a dry Earth atmosphere with pN_2 of 0.8 bars and pCO_2 of 0.5 bars at the surface and in a dry Martian atmosphere with pCO_2 of 1 bar at the surface. In addition, for these base terrestrial and Martian cases we examined the radiative effect from H_2O vapor at a constant relative humidity of 20%, 50% and 80%. The results for Earth and Mars are summarized in Figures 5 and 6, respectively. As expected, the parameterizations with the most opaque CO_2 window regions are the least sensitive to the addition of other greenhouse gases. For example, adding 10 ppmv SO_2 to a 1 bar pure CO_2 Martian atmosphere under the CA parameterization results in additional positive radiative forcing of about 26.0 W m^{-2}, while the same amount of SO_2 provides an additional 25.5 W m^{-2} under the MTCKD parameterization and only 18.3 W m^{-2} under the GBKM parameterization.

[52] We varied the oxygen isotopic composition of a dry Earth atmosphere containing 0.5 bars CO_2 and 0.8 bars N_2 and a dry Martian atmosphere with 1 bar CO_2 and found the effect to be small. We prescribed $^{18}O/^{16}O$ to be 1.025 and 1.050 times the present ratio in Earth's atmosphere and $^{17}O/^{16}O$ to be 1.013 and 1.025 times the present ratio, assuming the enrichment to be mass-dependent and despite evidence that some early materials formed in the solar system deviate from a mass-dependent relationship [see *Mittlefehldt et al.*, 2008, and references therein]. This changes the relative abundance of the different CO_2 isotopologues, including the asymmetric isotopologues, which have relatively strong lines between 1200 and 1450 cm^{-1}, in the CO_2 window regions. For the Earth simulations, the maximal additional radiative forcing (under the CA parameterization) was only 0.07 and 0.14 W m^{-2} for $^{18}O/^{16}O$ 1.025 and 1.050 times present Earth's, respectively. For the Mars simulations, the maximal additional forcing was 0.05 and 0.10 W m^{-2} for $^{18}O/^{16}O$ 1.025 and 1.050 times present Earth's, respectively. These differences are smaller than the model error.

4. Discussion

4.1. Comparison of CO_2 Line and Continuum Parameterizations

[53] As shown in the Results (Figure 3c), the difference in the OLR computed under the three different parameter combinations grows with increasing pCO_2 in the range considered here. The reason for this is that absorption by the lines is saturated even for relatively modest values of pCO_2 and the window regions become increasingly important for escape of radiation from the planet as pCO_2 is increased. Because the parameterizations differ primarily in the way absorption is formulated in the CO_2 window regions (continuum absorption), this results in a divergence in the computed OLR.

[54] The influence of the formulation of absorption in the window regions on atmospheric opacity is illustrated in Figures 4a–4c, where in the pure CO_2 case the differences in κ calculated with the three parameter combinations (panel a) affect the radiating temperature of the window regions, shown in panel b. The formulation of the continuum in the GBKM parameterization results in an extremely opaque atmosphere in the frequency region below 500 cm^{-1}, which radiates at a temperature close to the stratospheric temperature (T_{rad} = 160 K). Over the same frequency region, both the CA and MTCKD parameterizations result in transparent atmospheres and radiate at the surface temperature (T_{rad} = 273 K). Similarly, the differences in κ in the frequency region between 1200 and 1800 cm^{-1} result in a much more opaque atmosphere with the GBKM parameterization than with the other two (much lower T_{rad}).

[55] These differences in the opacity of the atmosphere lead to differences in the rate at which OLR accumulates during integration over frequency between 0 and 2500 cm^{-1} and in the resulting total OLR. Panel c shows that over half of the OLR is emitted at frequencies lower than 500 cm^{-1}, where the GBKM parameterization produces a very opaque atmosphere, leading to a total OLR from this region about 10 W m^{-2} lower than the other two parameterizations. At frequencies between 1200 and 1800 cm^{-1} the differences in opacity cause the difference in OLR between the CA and GBKM parameterizations to increase to almost ~28 W m^{-2}.

[56] The absorption coefficients calculated with the CA and MTCKD parameterizations differ by as much as five orders of magnitude in the spectral range between 1200 and 1800 cm^{-1} (Figure 4a). However, the coefficients under both parameterizations are low enough so that the atmosphere is essentially transparent and almost all of the infrared radiation escapes, resulting in little divergence in OLR between these parameterizations in this region of the spectrum (Figure 4c). The ~8 W m^{-2} difference between the CA and MTCKD parameterizations is accumulated almost entirely between 800 and 1000 cm^{-1}, where the differences in κ and opacity are seemingly small. The reasons are that this spectral region is important to emission at 273 K and that the values of κ are high enough to impact the transmission of radiation.

[57] When water is included (Figures 4d–4f) almost none of the difference in total OLR is accumulated at frequencies below 500 cm^{-1} or above 1500 cm^{-1}, where absorption by H_2O significantly increases the atmospheric opacity and reduces the sensitivity to the parameterization of absorption by CO_2. The radiating temperature and cumulative OLR reflect this, with a total OLR difference between the CA and GBKM parameterization of only ~13 W m^{-2} in the moist case (instead of ~28 W m^{-2} in the dry case), most of which is accumulated between 1200 and 1500 cm^{-1} with hardly any contribution below 500 cm^{-1} or above 1500 cm^{-1}.

[58] In addition to the sensitivity of the results to formulation of the continuum, we find that while the CA and GBKM parameterizations are sensitive to the choice of χ factor, the MTCKD parameterization is not (see Results). The reason for this is that in the CA and GBKM parameterizations absorption by the lines is computed out to a distance of 1000 and 500 cm^{-1}, respectively, and in some regions of the spectrum (e.g., 300–500 cm^{-1} and 750–900 cm^{-1}) the absorption is almost entirely due to the far wings of strong lines (Figure 4a). This means that the opacity in these important regions strongly depends on the choice of χ factor. On the other hand, in the MTCKD

parameterization the choice of χ factor affects the absorption out to only 25 cm^{-1} from the line centers, where a CO_2-rich atmosphere is opaque regardless of the χ factor and transmission is negligible. It is important to note, however, that in the MTCKD parameterization we calculate the CO_2 continuum from values tabulated in LBLRTM, but don't actually recalculate these values when changing the χ factor. The expectation is that if these values were recalculated with a different χ factor then the resulting continuum would differ, making the MTCKD parameterization as sensitive to the choice of χ factor as the others.

[59] Overall, it is clear that the formulation of absorption by CO_2 exerts an important control over the simulated opacity of CO_2-rich atmospheres. The largest differences in OLR and, though not included in this study, also in the infrared cooling rates and consequently the $p-T$ structure, arise from the way in which absorption in the CO_2 window regions is calculated (continuum absorption). Smaller but still significant differences arise from the formulation of the χ factor, though this parameter is not independent of the choice of continuum. Overcoming these difficulties will require experimental studies of self-broadened CO_2 absorption under the conditions relevant to early Earth and Mars.

4.2. Other Infrared Absorbers

[60] As previously mentioned, the parameterization of absorption by CO_2 importantly affects the sensitivity of LBL calculations to additional trace infrared absorbers. The magnitude of the additional forcing due to the presence of a greenhouse gas other than CO_2, as well as the difference in sensitivity to other greenhouse gases between the three parameterizations (Figures 5 and 6), strongly depend on the frequencies at which the greenhouse gas absorbs. This can be seen by comparing Figures 6a and 6c. The GBKM parameterization seems to be much less sensitive to addition of H_2O than the CA or MTCKD parameterizations. The reason for this is that H_2O vapor increases the opacity of the latter two parameterizations significantly below 500 cm^{-1} and between 1200 and 1800 cm^{-1} but only marginally for the GBKM parameterization, which is already relatively opaque in these frequency regions (see Figure 4d). SO_2, on the other hand, absorbs strongly between 450 and 600 cm^{-1}, where the absorption is relatively weak under all three parameterizations. As a result, the response to SO_2 is more uniform between the parameterizations, though the more opaque GBKM parameterization is still significantly less sensitive because absorption by SO_2 between 1100 and 1250 cm^{-1} is not as important as it is for the other two parameterizations.

[61] Out of all the greenhouse gases examined (other than H_2O) the OLR in a CO_2-rich atmosphere is found to be most sensitive to addition of NH_3 and SO_2 (Figures 5 and 6). At relatively low concentrations (1–10 ppmv) SO_2 provides stronger additional positive forcing, while at higher concentrations (100–1000 ppmv) the SO_2 bands become saturated and NH_3, which has more evenly distributed transitions in the thermal infrared region, has a stronger radiative effect. The weakest of the greenhouse gases is CH_4, especially under the GBKM parameterization. The reason is that CH_4 absorbs relatively weakly below 500 cm^{-1} and more strongly between 1200 and 1600 cm^{-1}, regions where CO_2 continuum absorption is strong under the GBKM parameterization.

[62] The sensitivity of the pure CO_2 atmosphere to the added greenhouse gases is somewhat misleading because H_2O vapor, which is a component of any realistic atmosphere, is absent from the calculations. A greenhouse containing both CO_2 and H_2O vapor would be less sensitive to addition of gases whose absorption overlaps with that of water, such as NH_3 and CH_4. Comparing SO_2 and NH_3, for example, in a moist atmosphere we find that SO_2 provides stronger radiative forcing up to concentrations of about 100 ppmv, above which the gases are comparable. In a pure CO_2 atmosphere, however, SO_2 is a more effective addition only up to a concentration of about 10 ppmv, above which NH_3 provides stronger forcing (Figures 5b–5c).

[63] The oxygen isotopic composition of CO_2 was found to be unimportant for $^{18}O/^{16}O$ as high as 1.050 times the ratio in the present Earth's atmosphere. Much higher values of early $^{18}O/^{16}O$ in the solar system can probably be precluded because the maximal ^{18}O enrichment observed in terrestrial planet and meteoritic material is ~25‰ (permil or part per thousand), corresponding to $^{18}O/^{16}O$ 1.025 times present Earth's [*Mittlefehldt et al.*, 2008]. Systems surrounding other stars, however, may have started with higher $^{18}O/^{16}O$, requiring that the effect of CO_2 isotopologue abundance on planetary climate be taken into consideration.

4.3. Importance of the Surface Albedo

[64] As mentioned, the surface albedo is a poorly constrained property, but one that is extremely important for the planetary energy budget. This importance is somewhat diminished in thick atmospheres because scattering by gas molecules may come to dominate the planetary albedo, which by analogy to the surface albedo is the reflectivity of the entire planet and depends on both the surface albedo and the atmospheric albedo. This is especially true when CO_2 concentrations are high because CO_2 is about 1.5 times as efficient a scatterer per unit mass as N_2. Thus, when pCO_2 is high, changes in the surface albedo matter less than they would at lower pCO_2 because less solar energy reaches the surface. For example, a purely scattering Martian atmosphere containing half a bar of CO_2 over a surface with a spectrally invariant albedo of 0.2 results in a planetary albedo of ~0.31. Increasing the surface albedo to 0.3 causes the planetary albedo to increase to ~0.40. The same change in the surface albedo under a 2 bar CO_2 atmosphere causes the planetary albedo to increase from ~0.42 to ~0.49. In the first case, the difference in the amount of solar energy absorbed by the planet between the low and high albedo scenarios is ~10 W m^{-2}, while in the second case it is only ~8 W m^{-2}, assuming the Sun was 75% its present luminosity. This is still a large difference in solar input, enforcing the importance of the surface albedo, although at higher values of pCO_2 this importance is diminished further.

[65] The importance of the surface albedo is accentuated for more modest values of pCO_2, such as those required to escape the global glaciations that occurred in the Neoproterozoic [*Kirschvink*, 1992; *Hoffman et al.*, 1998]. As mentioned in the introduction, the reflectivity of the snow and ice that covered Earth's surface is not well known and may have had values between 0.5 and 0.9 [*Warren et al.*,

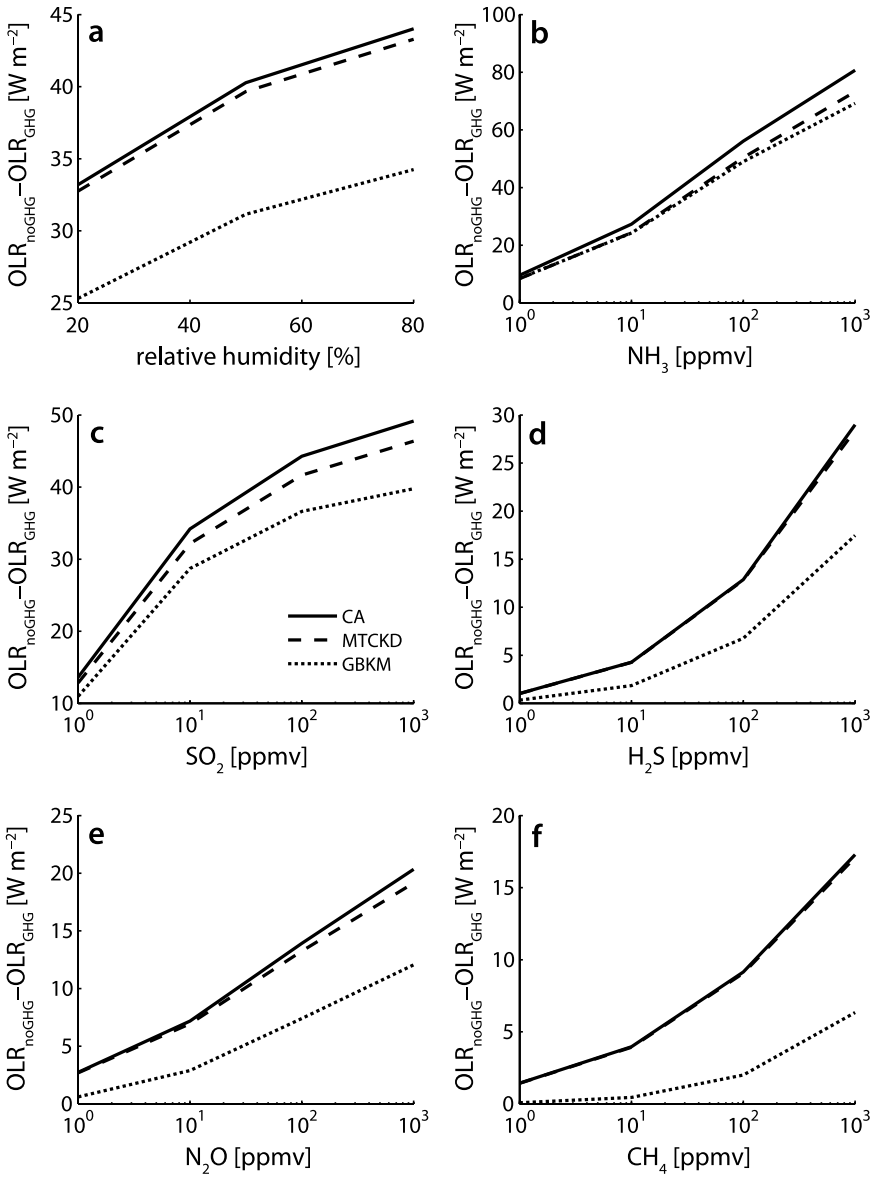

Figure 5. The net impact of adding greenhouse gases other than CO_2 (the difference in OLR between a dry reference Earth atmosphere with pCO_2 of 0.5 bars and pN_2 of 0.8 bars at the surface and the same atmosphere with the addition of other greenhouse gases). (a) Added radiative effect from H_2O vapor at 20%, 50% and 80% RH, constant with altitude. (b–f) Added radiative effect from 1, 10, 100, and 1000 ppmv of NH_3, SO_2, H_2S, N_2O, and CH_4, respectively.

2002]. To demonstrate the importance of the surface albedo to deglaciating a Neoproterozoic snowball, let us consider a purely scattering atmosphere containing 0.2 bars of CO_2 and 0.8 bars of N_2, over a global surface with a spectrally invariant albedo of either 0.6 or 0.8, well within the range of this very poorly constrained parameter. The corresponding planetary albedo is then ~0.67 or ~0.86, respectively and the absorbed solar energy, assuming the Sun was 94% its present luminosity as it was in the Neoproterozoic, is ~105 W m^{-2} or ~45 W m^{-2}, respectively. This difference of ~60 W m^{-2} between a snowball with a surface albedo of 0.6 and 0.8 puts into perspective the debate whether 0.1 or 0.3 bars of CO_2 were required to permit the deglaciation, considering that the difference in infrared radiative forcing due to such a tripling of pCO_2 is less than 20 W m^{-2}.

4.4. Implications for Early Planetary Climate

[66] We show above that differences in the formulation of absorption by CO_2, which produce similar atmospheric opacities at low CO_2 abundances, result in very large differences in radiative forcing by 0.1–5 bars of CO_2. Despite this uncertainty, a few implications arise for early planetary climate. For the case of Mars during the Noachian, while the three parameter combinations chosen here yield divergent results, none of them bring the surface T close to the melting point of H_2O; for all parameterizations the OLR at a surface T of 273 K is always greater than the absorbed solar flux (by ~40–60 W m^{-2}, depending on the parameterization). A parameterization similar to GBKM, for which CO_2 absorbs most strongly, together with a relatively strongly absorbing parameterization of H_2O vapor, was

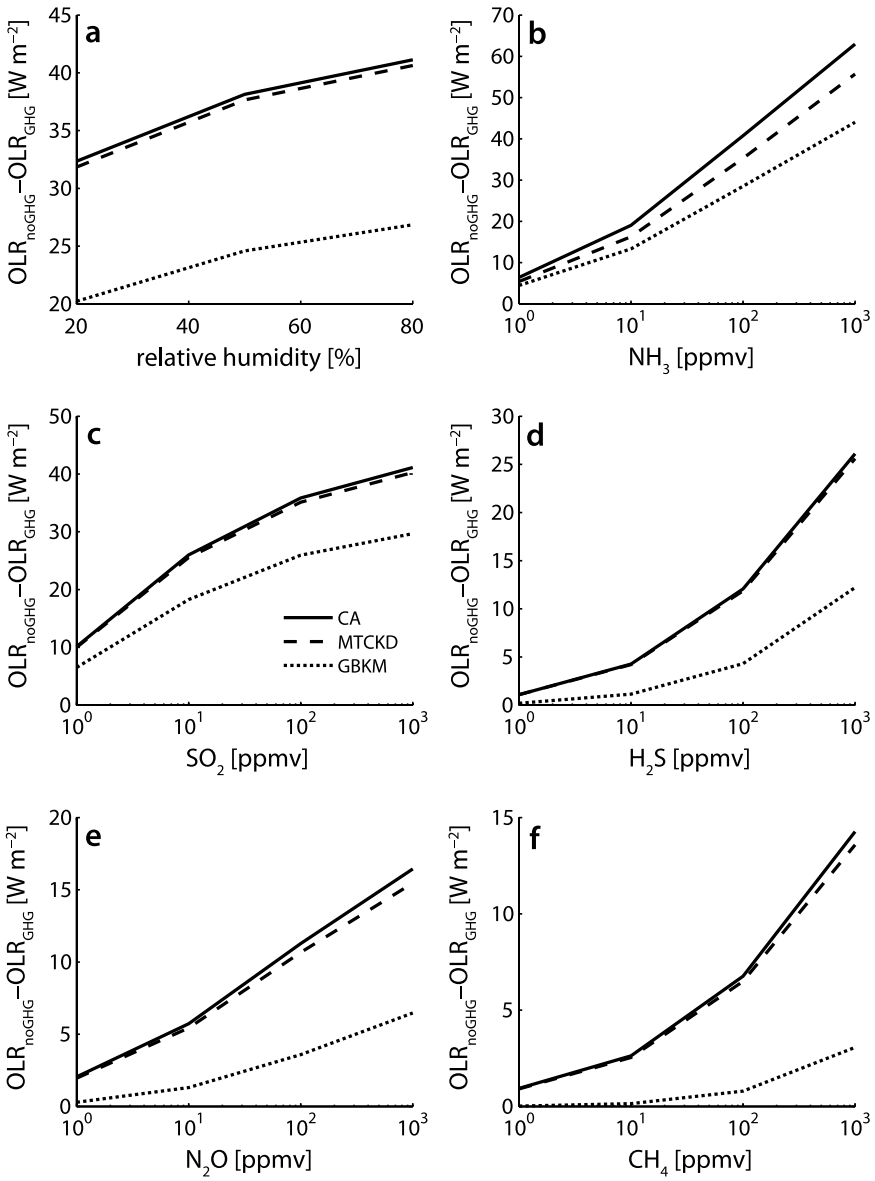

Figure 6. The net impact of adding greenhouse gases other than CO_2 (the difference in OLR between a dry reference Martian atmosphere with pCO_2 of 1 bar at the surface and the same atmosphere with the addition of other greenhouse gases). (a) Added radiative effect from H_2O vapor at 20%, 50% and 80% RH, constant with altitude. (b–f) Added radiative effect from 1, 10, 100, and 1000 ppmv of NH_3, SO_2, H_2S, N_2O, and CH_4, respectively.

used by *Kasting* [1991] to demonstrate that a CO_2-H_2O atmosphere was incapable on its own of getting the surface T to 273 K because of condensation of CO_2 and Rayleigh scattering by gaseous CO_2. Though future experimental work may find that even this is an underestimation of absorption by CO_2, the failure to reach super-freezing T using the most favorable of the currently existing parameterizations reinforces the notion that other infrared absorbers are required if the periods of surface runoff indicated by geomorphology and mineralogy were indeed the result of a more optically thick atmosphere.

[67] It would have been difficult for CH_4 and NH_3 to accumulate to radiatively important concentrations, given their susceptibility to photolysis and their relatively weak nonbiological sources on the terrestrial planets. CO_2-ice clouds, on the other hand, are expected to condense from a cold, CO_2-rich atmosphere and may provide a net positive forcing under a range of dynamical and microphysical conditions [*Forget and Pierrehumbert*, 1997; *Mischna et al.*, 2000; *Colaprete et al.*, 2003]. Another possibility is that SO_2, which based on the sulfur enrichment of Martian soils seems to have been an abundant component of early volcanic emissions [*Clark et al.*, 1976; *Yen et al.*, 2005], provided the additional radiative forcing. There are indications that under the anoxic, CO_2-rich conditions of the early Martian atmosphere, the lifetime of SO_2 was sufficiently increased relative to that of reflective H_2SO_4 aerosols, so that volcanic emission of SO_2 provided a net positive radiative forcing, unlike in the modern oxidizing Earth's atmosphere [*Johnson et al.*, 2009; *Levine and Summers*,

2008]. Under these conditions a negative climate feedback involving the atmospheric concentration of SO_2 and the rate of silicate weathering may have regulated the early climate of Mars [*Halevy et al.*, 2007], analogous to the CO_2 negative climate feedback on the modern Earth [*Walker et al.*, 1981].

[68] Adding 100 ppmv of SO_2 to a 1 bar CO_2 atmosphere with a relative humidity of 80% reduces the OLR by ~23–31 W m^{-2}, depending on the parameterization of CO_2 absorption. The OLR reduction alone is the radiative forcing equivalent of a doubling to a tripling of pCO_2 (Figures 3a–3b), but instead of involving the increase in planetary albedo due to Rayleigh scattering that would accompany such an increase in pCO_2, the planetary albedo actually decreases from ~0.33 to ~0.29 because of near-infrared and ultraviolet absorption of sunlight by SO_2. The difference between the OLR (at T_s = 273 K) and the solar radiation absorbed by the planet decreases from ~41–63 to ~17–23 W m^{-2}, depending on the parameterization of CO_2 absorption. Accompanying such high concentrations of SO_2, sulfuric acid aerosols are also expected to be relatively abundant and to counter some of the positive forcing by SO_2. The detailed atmospheric chemistry required to determine the concentration of sulfuric acid aerosols is beyond the scope of this paper and their radiative effect has not been included in the calculations. The resulting upper limit on the global average surface temperature, though highly uncertain because of the demonstrated uncertainty in absorption by CO_2, is around 250 K and low-latitude temperatures would likely come close to the freezing point of water or at times exceed it. Some of the mineral assemblages on the Martian surface precipitated from highly concentrated solutions [*Tosca et al.*, 2008], which have a lower freezing temperature than pure water. This implies that a global average surface temperature of about 250 K could have been enough to maintain substantial amounts of liquid at the surface, not only near the equator, potentially explaining the geomorphological evidence for surface runoff.

[69] As for the early Earth, the uncertainty in absorption by CO_2 shown here in combination with the uncertainty in the upper limits on paleo-pCO_2 estimates, mean that we cannot at present say whether infrared absorbers other than CO_2 and H_2O vapor were ever necessary to explain the persistence of liquid water despite a less luminous Sun. Other greenhouse gases, such as CH_4 and N_2O had significant biological sources going back perhaps billions of years and probably played some radiative role, although exactly how much remains unclear. Because the atmospheric concentrations of greenhouse gases other than CO_2 depend on their rates of production and destruction rather than on the abundance of CO_2, these gases may have existed in larger amounts than those required to supplement a CO_2-rich greenhouse. This would not have resulted in warmer surface temperatures because the CO_2–silicate weathering negative climate feedback would have driven pCO_2 down to the levels required for the temperature-dependent silicate weathering rates to balance volcanic outgassing of CO_2 by precipitation and burial of calcium carbonate [*Walker et al.*, 1981]. Thus, putting aside the error in the estimation methods, the paleo-pCO_2 estimates may be informing us of either (1) our inability to precisely calculate the radiative effect of CO_2-H_2O mixtures, which is not surprising given the work presented here or (2) the importance of other greenhouse gases relative to CO_2.

5. Conclusions

[70] We have shown that different parameterizations of line and continuum absorption by CO_2, which have been successful in simulating the present atmospheres of Earth, Mars and Venus, yield differences in outgoing longwave radiation of over 40 W m^{-2} when applied to the conditions relevant to the early history of Earth and Mars. This uncertainty in absorption by CO_2 pervades any climate modeling approach that utilizes the results of LBL calculations, which is to say all climate modeling approaches. With respect to the outstanding questions listed in the introduction to this paper, there are several implications.

[71] First, no credible estimate of the amount of CO_2 (in addition to H_2O vapor) required for liquid surface water on either early Earth or Mars can be made at present. Assessing whether other infrared absorbers or scatterers may have been required is likewise hindered. A solution to this will require laboratory measurements of self-broadened absorption by CO_2 over the relevant ranges of pressure, temperature and frequency, as well as measurements of CO_2-broadened absorption by H_2O vapor, though recent progress has been made in the case of the latter [*Brown et al.*, 2007]. Despite this uncertainty in the absorption by CO_2 and H_2O, the fact that the currently most opaque parameterization of CO_2 absorption cannot bring the surface of early Mars above the freezing point of water may suggest that additional infrared absorbers or scatterers were required. For the majority of Earth's history it is not clear that this is the case, that is, a CO_2-H_2O greenhouse may have been sufficient to keep the Earth's surface temperature above freezing. This is not to say that other infrared absorbers did not play a role, only that we cannot presently say whether they were ever a necessary condition for liquid water on the Earth's surface.

[72] Second, the surface albedo is an important property for the planetary energy budget and one which is at least as ill-constrained as the atmospheric abundance of infrared absorbers or scatterers. Unlike gaseous absorption, this cannot be addressed by laboratory measurements and will remain a factor of uncertainty in modeling studies of early paleoclimate. This is especially true for escape from the Proterozoic global glaciations; it is much easier to deglaciate a dirty snowball, in keeping with constraints on the duration of glaciation and the accumulation rate of CO_2, than it is a clean one.

[73] **Acknowledgments.** We thank three anonymous reviewers for comments that improved this work. I.H. was supported by a Harvard Origins of Life Initiative Graduate Fellowship, R. T. P. was funded by the National Science Foundation under grant ATM-0121028 and D. P. S. thanks Henry and Wendy Breck for their support.

References

Appel, P. W. U., C. M. Fedo, S. Moorbath, and J. S. Myers (1998), Recognizable primary volcanic and sedimentary features in a low-strain domain of the highly deformed, oldest known (~3.7–3.8 Gyr) Greenstone Belt, Isua, West Greenland, *Terra Nova*, *10*, 57–62.

Armstrong, R. L. (1982), Line mixing in the ν_2 band of CO_2, *Appl. Opt.*, *21*(12), 2141–2145.

Baker, V. R. (2001), Water and the Martian landscape, *Nature*, *412*(6843), 228–236.

Baker, V. R., M. H. Carr, V. C. Gulick, C. R. Williams, and M. S. Marley (1992), Channels and valley networks, in *Mars*, edited by H. Kieffer et al., pp. 493–522, Univ. of Ariz. Press, Tucson, Ariz.

Bandfield, J. L. (2002), Global mineral distributions on Mars, *J. Geophys. Res.*, *107*(E6), 5042, doi:10.1029/2001JE001510.

Bezard, B., C. Debergh, D. Crisp, and J. P. Maillard (1990), The deep atmosphere of Venus revealed by high-resolution nightside spectra, *Nature*, *345*(6275), 508–511.

Bishop, J. L., et al. (2008), Phyllosilicate diversity and past aqueous activity revealed at Mawrth Vallis, Mars, *Science*, *321*(5890), 830–833.

Boissoles, J., R. H. Tipping, and C. Boulet (1994), Theoretical study of the collision-induced fundamental absorption spectra of N_2–N_2 pairs for temperatures between 77 and 297 K, *J. Quant. Spectrosc. Radiat. Transfer*, *51*(4), 615–627.

Boissoles, J., C. Boulet, R. H. Tipping, A. Brown, and Q. Ma (2003), Theoretical calculation of the translation-rotation collision-induced absorption in N_2–N_2, O_2–O_2 and N_2–O_2 pairs, *J. Quant. Spectrosc. Radiat. Transfer*, *82*(1–4), 505–516.

Brown, L. R., C. M. Humphrey, and R. R. Gamache (2007), CO_2-broadened water in the pure rotation and ν_2 fundamental regions, *J. Mol. Spectrosc.*, *246*(1), 1–21.

Burch, D. E., and D. A. Gryvnak (1971), Absorption of infrared radiant energy by CO_2 and H_2O.5. absorption by CO_2 between 1100 and 1835 cm^{-1} (9.1–5.5 μm), *J. Opt. Soc. Am.*, *61*(4), 499.

Burch, D. E., D. A. Gryvnak, and D. Williams (1962), Total absorptance of carbon dioxide in the infrared, *Appl. Opt.*, *1*(6), 759–765.

Burch, D. E., D. A. Gryvnak, R. R. Patty, and C. E. Bartky (1969), Absorption of infrared radiant energy by CO_2 and H_2O.4. shapes of collision-broadened CO_2 lines, *J. Opt. Soc. Am.*, *59*(3), 267.

Cavosie, A. J., J. W. Valley, and S. A. Wilde (2005), Magmatic $\delta^{18}O$ in 4400–3900 Ma detrital zircons: A record of the alteration and recycling of crust in the early Archean, *Earth Planet. Sci. Lett.*, *235*(3–4), 663–681.

Clark, B. C., A. K. Baird, H. J. Rose, P. Toulmin, K. Keil, A. J. Castro, W. C. Kelliher, C. D. Rowe, and P. H. Evans (1976), Inorganic analyses of Martian surface samples at Viking landing sites, *Science*, *194*(4271), 1283–1288.

Clough, S. A., F. X. Kneizys, and R. W. Davies (1989), Line shape and the water vapor continuum, *Atmos. Res.*, *23*, 229–241.

Clough, S. A., M. W. Shephard, E. J. Mlawer, J. S. Delamere, M. J. Iacono, K. Cady-Pereira, S. Boukabara, and P. D. Brown (2005), Atmospheric radiative transfer modeling: a summary of the AER codes, *J. Quant. Spectrosc. Radiat. Transfer*, *91*(2), 233–244.

Colaprete, A., R. M. Haberle, and O. B. Toon (2003), Formation of convective carbon dioxide clouds near the south pole of Mars, *J. Geophys. Res.*, *108*(E7), 5081, doi:10.1029/2003JE002053.

Craddock, R. A., and T. A. Maxwell (1993), Geomorphic evolution of the Martian highlands through ancient fluvial processes, *J. Geophys. Res.*, *98*(E2), 3453–3468.

Ellingson, R. G., J. Ellis, and S. B. Fels (1991), The intercomparison of radiation codes used in climate models: Long-wave results, *J. Geophys. Res.*, *96*(D5), 8929–8953.

Emanuel, K. A., and M. Zivkovic-Rothman (1999), Development and evaluation of a convection scheme for use in climate models, *J. Atmos. Sci.*, *56*(11), 1766–1782.

Emmanuel, S., and J. J. Ague (2007), Implications of present-day abiogenic methane fluxes for the early Archean atmosphere, *Geophys. Res. Lett.*, *34*, L15810, doi:10.1029/2007GL030532.

Fanale, F. P., S. E. Postawko, J. B. Pollack, and M. H. Carr (1992), Mars: Epochal climate change and volatile history, in *Mars*, edited by H. Kieffer et al., pp. 1135–1179, Univ. of Ariz. Press, Tucson, Ariz.

Fassett, C. I., and J. W. Head (2008a), The timing of Martian valley network activity: Constraints from buffered crater counting, *Icarus*, *195*(1), 61–89.

Fassett, C. I., and J. W. Head (2008b), Valley network-fed, open-basin lakes on Mars: Distribution and implications for Noachian surface and subsurface hydrology, *Icarus*, *198*(1), 37–56.

Fels, S. B. (1979), Simple strategies for inclusion of Voigt effects in infrared cooling rate calculations, *Appl. Opt.*, *18*(15), 2634–2637.

Fenton, L. K., P. E. Geissler, and R. M. Haberle (2007), Global warming and climate forcing by recent albedo changes on Mars, *Nature*, *446*(7136), 646–649.

Forget, F., and R. T. Pierrehumbert (1997), Warming early Mars with carbon dioxide clouds that scatter infrared radiation, *Science*, *278*(5341), 1273–1276.

Forster, P. M. D., and K. E. Taylor (2006), Climate forcings and climate sensitivities diagnosed from coupled climate model integrations, *J. Clim.*, *19*(23), 6181–6194.

Frommhold, L. (1993), *Collision-Induced Absorption in Gases*, Cambridge Univ. Press, Cambridge, U. K.

Fukabori, M., T. Nakazawa, and M. Tanaka (1986), Absorption properties of infrared active gases at high-pressures: 1. CO_2, *J. Quant. Spectrosc. Radiat. Transfer*, *36*(3), 265–270.

Goldblatt, C., A. J. Matthews, T. M. Lenton, A. J. Watson, and K. Zahnle (2008), The global nitrogen budget and the faint young Sun paradox, *Eos Trans. AGU*, *89*(53), Fall Meet. Suppl., Abstract P33D-02.

Golombek, M. P., and N. T. Bridges (2000), Erosion rates on Mars and implications for climate change: Constraints from the Pathfinder landing site, *J. Geophys. Res.*, *105*(E1), 1841–1853.

Goody, R., R. West, L. Chen, and D. Crisp (1989), The correlated-k method for radiation calculations in nonhomogeneous atmospheres, *J. Quant. Spectrosc. Radiat. Transfer*, *42*(6), 539–550.

Gough, D. O. (1981), Solar interior structure and luminosity variations, *Sol. Phys.*, *74*, 21–34.

Gruszka, M., and A. Borysow (1996), New analysis of the spectral moments of collision induced absorption in gaseous N_2 and CO_2, *Mol. Phys.*, *88*(5), 1173–1185.

Gruszka, M., and A. Borysow (1997), Roto-translational collision-induced absorption of CO_2 for the atmosphere of Venus at frequencies from 0 to 250 cm^{-1}, at temperatures from 200 to 800 K, *Icarus*, *129*(1), 172–177.

Gruszka, M., and A. Borysow (1998), Computer simulation of the far infrared collision induced absorption spectra of gaseous CO_2, *Mol. Phys.*, *93*(6), 1007–1016.

Halevy, I., M. T. Zuber, and D. P. Schrag (2007), A sulfur dioxide climate feedback on early Mars, *Science*, *318*, 1903–1907.

Haqq-Misra, J. D., S. D. Domagal-Goldman, P. J. Kasting, and J. F. Kasting (2008), A revised, hazy methane greenhouse for the Archean Earth, *Astrobiology*, *8*(5), 1127–1137.

Hessler, A. M., D. R. Lowe, R. L. Jones, and D. K. Bird (2004), A lower limit for atmospheric carbon dioxide levels 3.2 billion years ago, *Nature*, *428*(6984), 736–738.

Ho, W., G. Birnbaum, and A. Rosenberg (1971), Far-infrared collision-induced absorption in CO_2: 1. Temperature dependence, *J. Chem. Phys.*, *55*(3), 1028.

Hoffman, P. F., A. J. Kaufman, G. P. Halverson, and D. P. Schrag (1998), A Neoproterozoic snowball Earth, *Science*, *281*(5381), 1342–1346.

Ingersol, A. P. (1969), Runaway greenhouse: A history of water on Venus, *J. Atmos. Sci.*, *26*(6), 1197.

IPCC (2007), *Climate Change 2007: The Physical Science Basis. Contribution of Working Group I to the Fourth Assessment Report of the Intergovernmental Panel on Climate Change*, edited by S. Solomon et al., 996 pp., Cambridge Univ. Press, Cambridge, U. K.

Johnson, S. S., M. A. Mischna, T. L. Grove, and M. T. Zuber (2008), Sulfur-induced greenhouse warming on early Mars, *J. Geophys. Res.*, *113*, E08005, doi:10.1029/2007JE002962.

Johnson, S. S., A. A. Pavlov, and M. A. Mischna (2009), The fate of SO_2 in the ancient Martian atmosphere: Implications for transient greenhouse warming, *J. Geophys. Res.*, doi:10.1029/2008JE003313, in press.

Kah, L. C., and R. Riding (2007), Mesoproterozoic carbon dioxide levels inferred from calcified cyanobacteria, *Geology*, *35*(9), 799–802.

Kasting, J. F. (1982), Stability of ammonia in the primitive terrestrial atmosphere, *J. Geophys. Res.*, *87*(C4), 3091–3098.

Kasting, J. F. (1987), Theoretical constraints on oxygen and carbon-dioxide concentrations in the Precambrian atmosphere, *Precambrian Res.*, *34*(3–4), 205–229.

Kasting, J. F. (1988), Runaway and moist greenhouse atmospheres and the evolution of Earth and Venus, *Icarus*, *74*(3), 472–494.

Kasting, J. F. (1991), CO_2 condensation and the climate of early Mars, *Icarus*, *94*(1), 1–13.

Kasting, J. F. (1997), Planetary atmospheres: Warming early Earth and Mars, *Science*, *276*(5316), 1213–1215.

Kasting, J. F., J. B. Pollack, and T. P. Ackerman (1984a), Response of Earth's atmosphere to increases in solar flux and implications for loss of water from Venus, *Icarus*, *57*(3), 335–355.

Kasting, J. F., J. B. Pollack, and D. Crisp (1984b), Effects of high CO_2 levels on surface-temperature and atmospheric oxidation-state of the early Earth, *J. Atmos. Chem.*, *1*(4), 403–428.

Keller-Rudek, H., and G. K. Moortgat (2009), MPI-Mainz-UV–VIS Spectral Atlas of Gaseous Molecules. (Available at www.atmosphere.mpg.de/spectral-atlas-mainz)

Kiehl, J. T. (2007), Twentieth century climate model response and climate sensitivity, *Geophys. Res. Lett.*, *34*, L22710, doi:10.1029/2007GL031383.

Kirschvink, J. L. (1992), Late Proterozoic low-latitude global glaciation: The snowball Earth, in *The Proterozoic Biosphere*, edited by J. W. Schopf and C. Klein, 5152 pp., Cambridge Univ. Press, New York.

Kratz, D. P., M. G. Mlynczak, C. J. Mertens, H. Brindley, L. L. Gordley, J. Martin-Torres, F. M. Miskolczi, and D. D. Turner (2005), An intercomparison of far-infrared line-by-line radiative transfer models, *J. Quant. Spectrosc. Radiat. Transfer*, *90*, 323–341.

Kuhn, W. R., and S. K. Atreya (1979), Ammonia photolysis and the greenhouse effect in the primordial atmosphere of the Earth, *Icarus*, *37*(1), 207–213.

Lammer, H., H. I. M. Lichtenegger, C. Kolb, I. Ribas, E. F. Guinan, R. Abart, and S. J. Bauer (2003), Loss of water from Mars: Implications for the oxidation of the soil, *Icarus*, *165*(1), 9–25.

Lammer, H., J. F. Kasting, E. Chassefiere, R. E. Johnson, Y. N. Kulikov, and F. Tian (2008), Atmospheric escape and evolution of terrestrial planets and satellites, *Space Sci. Rev.*, *139*(1–4), 399–436.

Le Doucen, R., C. Cousin, C. Boulet, and A. Henry (1985), Temperature-dependence of the absorption in the region beyond the 4.3 μm band head of CO_2: 1. Pure CO_2 case, *Appl. Opt.*, *24*(6), 897–906.

Le Hir, G., G. Ramstein, Y. Donnadieu, and Y. Godderis (2008), Scenario for the evolution of atmospheric CO_2 during a snowball Earth, *Geology*, *36*(1), 47–50.

Levine, J., and M. Summers (2008), The impact of carbon dioxide on the composition and chemistry of the atmospheres of Earth and Mars, *Brown-Vernadsky Microsymp.*, *XXXXVII*.

Lide, D. R. (2006), *CRC Handbook of Chemistry and Physics*, 87th ed., CRC Press, Boca Raton, Fla.

Ma, Q. C., R. H. Tipping, C. Boulet, and J. P. Bouanich (1999), Theoretical far-wing line shape and absorption for high-temperature CO_2, *Appl. Opt.*, *38*(3), 599–604.

McKay, C. P., R. D. Lorenz, and J. I. Lunine (1999), Analytic solutions for the antigreenhouse effect: Titan and the early Earth, *Icarus*, *137*(1), 56–61.

Meadows, V. S., and D. Crisp (1996), Ground-based near-infrared observations of the Venus nightside: The thermal structure and water abundance near the surface, *J. Geophys. Res.*, *101*(E2), 4595–4622.

Melsheimer, C., et al. (2005), Intercomparison of general purpose clear sky atmospheric radiative transfer models for the millimeter/submillimeter spectral range, *Radio Sci.*, *40*, RS1007, doi:10.1029/2004RS003110.

Mischna, M. A., J. F. Kasting, A. Pavlov, and R. Freedman (2000), Influence of carbon dioxide clouds on early Martian climate, *Icarus*, *145*(2), 546–554.

Mittlefehldt, D. W., R. N. Clayton, M. J. Drake, and K. Righter (2008), Oxygen isotopic composition and chemical correlations in meteorites and the terrestrial planets, *Oxygen Sol. Syst.*, *68*, 399–428.

Mojzsis, S. J., T. M. Harrison, and R. T. Pidgeon (2001), Oxygen-isotope evidence from ancient zircons for liquid water at the Earth's surface 4,300 Myr ago, *Nature*, *409*(6817), 178–181.

Moore, J. F. (1971), Infrared absorption of carbon dioxide at high densities with application to the atmosphere of Venus, Ph.D. thesis, Columbia Univ. Press, New York.

Muehlenbachs, K. (1998), The oxygen isotopic composition of the oceans, sediments and the seafloor, *Chem. Geol.*, *145*, 263–273.

Newman, M. J., and R. T. Rood (1977), Implications of solar evolution for Earths early atmosphere, *Science*, *198*(4321), 1035–1037.

Niro, F., C. Boulet, and J. M. Hartmann (2004), Spectra calculations in central and wing regions of CO_2 IR bands: I. Model and laboratory measurements, *J. Quant. Spectrosc. Radiat. Transfer*, *88*(4), 483–498.

Niro, F., K. Jucks, and J. M. Hartmann (2005), Spectra calculations in central and wing regions of CO_2 IR bands: IV. Software and database for the computation of atmospheric spectra, *J. Quant. Spectrosc. Radiat. Transfer*, *95*(4), 469–481.

Pavlov, A. A., J. F. Kasting, L. L. Brown, K. A. Rages, and R. Freedman (2000), Greenhouse warming by CH_4 in the atmosphere of early Earth, *J. Geophys. Res.*, *105*(E5), 11,981–11,990.

Pavlov, A. A., L. L. Brown, and J. F. Kasting (2001), UV shielding of NH_3 and O_2 by organic hazes in the Archean atmosphere, *J. Geophys. Res.*, *106*(E10), 23,267–23,287.

Penner, S. S., and P. Varanasi (1967), Spectral absorption coefficients in pure rotation spectrum of water vapor, *J. Quant. Spectrosc. Radiat. Transfer*, *7*(4), 687.

Perrin, M. Y., and J. M. Hartmann (1989), Temperature-dependent measurements and modeling of absorption by CO_2–N_2 mixtures in the far line-wings of the 4.3 μm CO_2 band, *J. Quant. Spectrosc. Radiat. Transfer*, *42*(4), 311–317.

Phillips, P. J., et al. (2001), Ancient geodynamics and global-scale hydrology on Mars, *Science*, *291*(5513), 2587–2591.

Pickett, H. M., R. L. Poynter, E. A. Cohen, M. L. Delitsky, J. C. Pearson, and H. S. P. Muller (1998), Submillimeter, millimeter, and microwave spectral line catalog, *J. Quant. Spectrosc. Radiat. Transfer*, *60*(5), 883–890.

Pierrehumbert, R. T. (2005), Climate dynamics of a hard snowball Earth, *J. Geophys. Res.*, *110*, D01111, doi:10.1029/2004JD005162.

Pierrehumbert, R. T., H. Brogniez, and R. Roca (2007), On the relative humidity of the atmosphere, in *The Global Circulation of the Atmosphere*, edited by T. Schneider and A. Sobel, pp. 144–185, Princeton Univ. Press, Princeton, N. J.

Pollack, J. B. (1979), Climatic change on the terrestrial planets, *Icarus*, *37*(3), 479–553.

Pollack, J. B. (1991), Kuiper Prize lecture: Present and past climates of the terrestrial planets, *Icarus*, *91*(2), 173–198.

Pollack, J. B., J. F. Kasting, S. M. Richardson, and K. Poliakoff (1987), The case for a wet, warm climate on early Mars, *Icarus*, *71*(2), 203–224.

Postawko, S. E., and W. R. Kuhn (1986), Effect of the greenhouse gases (CO_2, H_2O, SO_2) on Martian paleoclimate, *J. Geophys. Res.*, *91*(B4), D431–D438.

Poulet, F., J. P. Bibring, J. F. Mustard, A. Gendrin, N. Mangold, Y. Langevin, R. E. Arvidson, B. Gondet, and C. Gomez (2005), Phyllosilicates on Mars and implications for early Martian climate, *Nature*, *438*(7068), 623–627.

Poulet, F., C. Gomez, J. P. Bibring, Y. Langevin, B. Gondet, P. Pinet, G. Belluci, and J. Mustard (2007), Martian surface mineralogy from Observatoire pour la Mineralogie, l'Eau, les Glaces et l'Activite on board the Mars Express spacecraft (OMEGA/MEx): Global mineral maps, *J. Geophys. Res.*, *112*, E08S02, doi:10.1029/2006JE002840.

Rothman, L. S., et al. (2005), The HITRAN 2004 molecular spectroscopic database, *J. Quant. Spectrosc. Radiat. Transfer*, *96*(2), 139–204.

Rye, R., P. H. Kuo, and H. D. Holland (1995), Atmospheric carbon-dioxide concentrations before 2.2-billion years ago, *Nature*, *378*(6557), 603–605.

Sagan, C. (1977), Reducing greenhouses and temperature history of Earth and Mars, *Nature*, *269*(5625), 224–226.

Sagan, C., and G. Mullen (1972), Earth and Mars: Evolution of atmospheres and surface temperatures, *Science*, *177*(4043), 52.

Segura, A., V. S. Meadows, J. F. Kasting, D. Crisp, and M. Cohen (2007), Abiotic formation of O_2 and O_3 in high-CO_2 terrestrial atmospheres, *Astron. Astrophys.*, *472*(2), 665–679.

Segura, T. L., O. B. Toon, and A. Colaprete (2008), Modeling the environmental effects of moderate-sized impacts on Mars, *J. Geophys. Res.*, *113*, E11007, doi:10.1029/2008JE003147.

Segura, T. L., O. B. Toon, A. Colaprete, and K. Zahnle (2002), Environmental effects of large impacts on Mars, *Science*, *298*(5600), 1977–1980.

Sheldon, N. D. (2006), Precambrian paleosols and atmospheric CO_2 levels, *Precambrian Res.*, *147*(1–2), 148–155.

Squyres, S. W., et al. (2004), In situ evidence for an ancient aqueous environment at Meridiani Planum, Mars, *Science*, *306*(5702), 1709–1714.

Tipping, R. H., and Q. Ma (1995), Theory of the water-vapor continuum and validations, *Atmos. Res.*, *36*(1–2), 69–94.

Tjemkes, S. A., et al. (2003), The ISSWG line-by-line inter-comparison experiment, *J. Quant. Spectrosc. Radiat. Transfer*, *77*, 433–453.

Tonkov, M. V., et al. (1996), Measurements and empirical modeling of pure CO_2 absorption in the 2.3 μm region at room temperature: Far wings, allowed and collision-induced bands, *Appl. Opt.*, *35*(24), 4863–4870.

Tosca, N. J., A. H. Knoll, and S. M. McLennan (2008), Water activity and the challenge for life on early Mars, *Science*, *320*(5880), 1204–1207.

Tvorogov, S. D., O. B. Rodimova, and L. I. Nesmelova (2005), On the correlated k-distribution approximation in atmospheric calculations, *Opt. Eng.*, *44*(7), 071202.

Valley, J. W., W. H. Peck, E. M. King, and S. A. Wilde (2002), A cool early Earth, *Geology*, *30*(4), 351–354.

Van Vleck, J. H., and D. L. Huber (1977), Absorption, emission, and linebreadths: Semi-historical perspective, *Rev. Mod. Phys.*, *49*(4), 939–959.

Van Vleck, J. H., and V. F. Weisskopf (1945), On the shape of collision-broadened lines, *Rev. Mod. Phys.*, *17*(2–3), 227–236.

von Paris, P., H. Rauer, J. L. Grenfell, B. Patzer, P. Hedelt, B. Stracke, T. Trautmann, and F. Schreier (2008), Warming the early Earth—CO_2 reconsidered, *Planet. Space Sci.*, *56*(9), 1244–1259.

Walker, J. C. G., P. B. Hays, and J. F. Kasting (1981), A negative feedback mechanism for the long-term stabilization of Earth's surface temperature, *J. Geophys. Res.*, *86*(C10), 9776–9782.

Warren, S. G., R. E. Brandt, T. C. Grenfell, and C. P. McKay (2002), Snowball Earth: Ice thickness on the tropical ocean, *J. Geophys. Res.*, *107*(C10), 3167, doi:10.1029/2001JC001123.

Wiscombe, W. J., and J. W. Evans (1977), Exponential-sum fitting of radiative transmission functions, *J. Comput. Phys.*, *24*(4), 416–444.

Yen, A. S., et al. (2005), An integrated view of the chemistry and mineralogy of Martian soils, *Nature*, *436*(7047), 49–54.

Yung, Y. L., H. Nair, and M. F. Gerstell (1997), CO_2 greenhouse in the early Martian atmosphere: SO_2 inhibits condensation, *Icarus*, *130*(1), 222–224.

Zahnle, K. J. (1993), Xenological constraints on the impact erosion of the early Martian atmosphere, *J. Geophys. Res.*, *98*(E6), 10,899–10,913.

I. Halevy and D. P. Schrag, Department of Earth and Planetary Sciences, Harvard University, 20 Oxford Street, Cambridge, MA 02138, USA. (ihalevy@fas.harvard.edu; schrag@eps.harvard.edu)

R. T. Pierrehumbert, Department of Geophysical Sciences, University of Chicago, 5734 South Ellis Avenue, Chicago, IL 60637, USA. (rtp1@geosci.uchicago.edu)